Modeling Metal-Catalyzed Olefin Polymerization

A. K. Rappé*

Department of Chemistry, Colorado State University, Fort Collins, Colorado 80523

W. M. Skiff

Bristol Bay Campus, University of Alaska, Fairbanks, Dillingham, Alaska 99576

C. J. Casewit

General Molecular Incorporated, 3951 Braidwood Drive, Fort Collins, Colorado 80524

Received September 2, 1999

Contents

I. Introduction

Research in single-center metal-catalyzed polymerization has seen explosive growth over the past two decades, advancing from questions of academic interest to solving problems in the commercial arena.[1] This growth has occurred in large measure due to ligand modification. Catalyst activities have increased 300-fold; current metallocene catalysts have turnover frequencies that rival those of enzymes. Stereocontrol of a hydrocarbon as simple as propylene is largely unmatched in organic synthesis.

Molecular models have played major roles in these activity and control advancements, particularly in the stereocontrol of propylene polymerization. Prominent examples include the Pino−Corradini active site model,[2,3] Ewen's active site symmetry model,[4] and Brookhart's agostically stabilized alkyl resting state[5] and olefin binding site blockage models.[6] The development of these seminal models has, in large part, relied only on the results of the simplest of computational technologies, the most useful tool being simple visualization. More elaborate technologies have to date been limited to a supporting role due to speed, accuracy, and system size challenges. On the basis of the work reviewed here, these limitations are rapidly diminishing.

A major challenge for theoretical modeling of metal-catalyzed polymerization is the choice of computational model system. Experimental studies use a catalyst precursor and an activator complex that generates a cationic active catalyst in solution[7−14] with a pendant weakly coordinating counteranion.[15] Unfortunately, supporting computational studies reviewed here have generally used a gas-phase cationic model. While there are ample data to suggest that polymerization is often independent of counteranion or solvent, there is a growing body of published experimental work wherein the choice of counteranion[16] or even solvent[17] changes the nature of the polymerization process. There have been scattered reports wherein a counteranion model has been included in the computational study[18−22] and a few papers that have incorporated limited solvation effects in the model.[18,20,22] Unfortunately, this work is the exception rather than the rule.

The commercial expansion of single-center polymerization has not occurred in a vacuum but at the expense of conventional heterogeneous Zielger−Natta polymerization.[23] Our understanding of single-center polymerization has also not occurred in a vacuum; active site conceptual models have evolved from heterogeneous Ziegler−Natta active site models.[4,24] This review will focus on modeling studies of single-center polymerization, though mention will be given of early studies that modeled the heterogeneous process.

10.1021/cr9902493 CCC: $35.00
Published on Web 03/08/2000

A. K. Rappé was born and raised in Okanogan, WA, and received his B.S. degree from the University of Puget Sound in 1974. He earned his doctorate from Caltech in 1981, working with Professor W. A. Goddard on olefin metathesis and hydrocarbon oxidation. Following postdoctoral work, Dr. Rappé joined Colorado State University. Dr. Rappé has used ab initio electronic structure and empirical force field technologies to study a number of organometallic reactions including nitrogen activation, deNOx catalysis, zeolite-based cracking, olefin metathesis and polymerization, and hydrocarbon oxidation. The Rappé group, in collaboration with Dr. Casewit of General Molecular and Dr. Skiff of the University of Alaska, has also worked on the development of force field technology (functional forms and parameters) for the entire periodic table as well as for chemical reactivity studies. This work has resulted in the universal force field (UFF), the reaction force field (RFF), and the first generation reaction potential method. Dr. Rappé has collaborated with chemists at the Big Three petrochemical companies and has served as a consultant for a number of other chemical firms. In 1991, and again in 1992, Dr. Rappé was a recipient of a Union Carbide Innovation Recognition Award.

W. M. Skiff received his doctorate in physical chemistry in 1985 from Arizona State University, working with Professors Ray W. Carpenter and Sheng H. Lin. His graduate research centered on analytical electron microscopy, where he specialized in both experimental and theoretical aspects of electron energy loss spectroscopy. Following postdoctoral research, Dr. Skiff joined Shell Oil Co. in Houston, TX, as a theoretical chemist in 1988. There he worked on a wide variety of problems in the petrochemical industry, particularly catalysis. Since joining Shell he has collaborated with A. K. Rappé on the development of force fields and computational tools. From 1994 to 1996 Dr. Skiff was a visiting scientist at Koninklijke/Shell-Laboratorium, Amsterdam. In 1999 Skiff joined the faculty at the Bristol Bay Campus of the University of Alaska, Fairbanks. As an assistant professor of chemistry, he has begun exploiting Java technology for distance learning. The goal of this work is to provide a real-time, interactive, virtual classroom for teaching sciences and mathematics. Dr. Skiff serves as Vice President of General Molecular Incorporated.

As reviewed elsewhere,[7−14] single-center olefin polymerization is a rather complex task. Typically, a well-defined organometallic complex is mixed with an activator complex, usually a Lewis acidic main-group organometallic complex, to generate an active catalytic system composed of a cationic metal complex and an anionic main-group complex. In the nonpolar polymerization medium, the cation and anion likely form an ion pair. The most common activator is known as MAO (methylalumoxane). MAO is a complex mixture of chemical species but has the rough C:Al:O stoichiometry of 1:1:1. MAO is prepared from the careful reaction of trimethylaluminum with water. MAO is thought to (1) replace chlorides from a dichloro precursor complex with methyls, (2) abstract a CH_3^- from the transition-metal complex, forming a weakly coordinating counteranion, and (3) scavenge or scrub impurities.

C. J. Casewit was born in Frankfurt, Germany, grew up in Colorado, and attended the University of Colorado at Denver, graduating with a B.A. in chemistry. She received her Ph.D. in 1981 from Caltech, where she carried out experimental research in physical organic chemistry under the direction of John D. Roberts. While at Caltech she begun a long-term collaboration with W. A. Goddard III and Anthony K. Rappé in theory. Dr. Casewit returned to Colorado, working on organometallic catalysis at the University of Colorado at Boulder. In 1988, she started research in the field of molecular mechanics, resulting in the development of the widely-used universal force field. She is co-author of the textbook *Molecular Mechanics across Chemistry*, published by University Science. Dr. Casewit serves as President of General Molecular Incorporated, a software company devoted to commercializing theoretical technology useful in modeling polymerization catalysis.

Once an active catalytic system is generated and exposed to olefin, polymerization proceeds through a chain reaction. As proposed by Cossee and Arlman[25] in 1964, the chain propagation cycle starts with a vacant coordination site and the coordination of an olefin to this vacant coordination site at the metal, eq 1. Olefin coordination is followed by the insertion

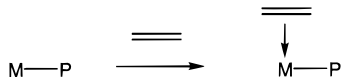

(1)

of the olefin π bond into the metal−carbon σ bond of the growing polymer chain, eq 2. Stereo- and regiocontrol of vinyl olefin polymerization is thought to occur at this stage. Despite its simplicity, this basic cycle has withstood 35 years of investigation.

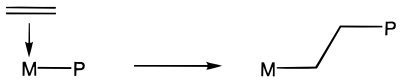

(2)

Chain termination can occur through a number of pathways. The growing polymer chain can transfer a β-hydrogen to the metal, eq 3, generating an olefin-

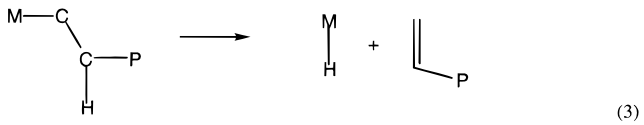

(3)

terminated polymer and a metal hydride complex. The metal hydride complex can undergo olefin insertion, initiating growth of a new polymer chain. The polymer chain can transfer a β-hydrogen to an incoming monomer, eq 4, again generating an olefin-

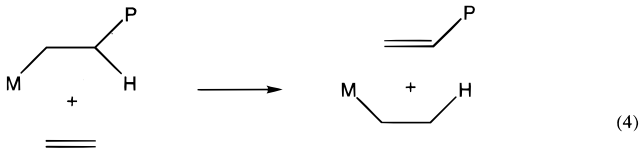

(4)

terminated polymer and a metal alkyl, which can initiate chain growth. The polymer chain can be transferred to the counteranion, eq 5, generating a

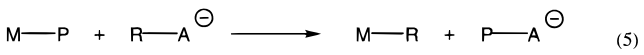

(5)

polymer "capped" by an organometallic functional group and a new cationic metal alkyl, which can initiate chain growth. Chain growth can also be stopped by the generation of catalytically inactive or dormant species or inactive sites. Often these inactive sites can be reactivated by the addition of hydrogen and, in the case of propylene polymerization, by the addition of ethylene.

Computational modeling studies of nearly all of these steps have been reported; this work will be reviewed in sections IV−VII. Experimental variables such as solvent, pressure, temperature control, and reaction scale all impact on observed polymer properties. Different research groups using the same catalyst have reported a range of results. The impact of these experimental variations in comparison with modeling studies is discussed in section II. Given the complexity of the olefin polymerization process, modeling studies have ranged from the rather simple to the quite elaborate; the theoretical approaches used are reviewed in section III. As mentioned above the model complexes used in the computational study of single-center olefin polymerization have their limitations; enhancements are discussed in section VIII.

II. Experimental Data

Elevated temperatures, ~70 °C, and enhanced pressures, 5−10 atm, are conventionally used for olefin polymerization. The catalytically active species is formed in situ from a catalyst precursor. The solvent medium changes during the course of reaction. Initially a solvent such as propylene or toluene surrounds the active site, but shortly the active site is encased in a polymeric solution. Seemingly insignificant changes in reaction medium perturb the observed polymeric properties. For these reasons, for modeling studies one must proceed with caution when using experimental data to provide rough estimates of validity.

Modeling studies can most straightforwardly calculate energy differences. These energy differences can be compared with estimates of rate ratios. For example, if a Shultz−Flory distribution[26] is assumed, then the molecular weight, either number-averaged (M_n) or weight-averaged (M_w), can provide a measure of propagation to termination rates. If the usual Shultz−Flory distribution is observed, then a polydispersity (M_w/M_n) of 2 is found. If propagation and termination have the same concentration dependence on the monomer, then the ratio of rates correlates with an activation energy difference. For propylene polymerization an M_w of 100 000 corresponds to a ratio of rates of 2400 and an activation energy difference of 4.8 kcal/mol at 70 °C. Doubling M_w only increases the energy difference by 0.5 kcal/mol. Increasing M_w to 1 000 000 increases the energy difference to 6.4 kcal/mol. For ethylene polymerization the corresponding activation energy differences are 5.1, 5.6, and 6.6 kcal/mol.

If propagation and termination differ in their monomer concentration dependence, the analysis is more challenging, and estimates of activation energy differences are more qualitative. At 70 °C liquid propylene has a density of roughly 0.5 g/L.[27] This leads to a propylene concentration of 10 M, which would uniformly raise the activation energy differences by 2.3 kcal/mol if polymerization were carried out under constant propylene pressure. On the other hand, if monomer is depleted during polymerization, M_w will reflect an "average" concentration. Roughly 99% of the polymer will be produced by the time the propylene concentration drops to 0.1 M. This suggests an average propylene concentration of 1 M, which would have no effect on our estimate of activation energy differences, but would cause a broadening in the molecular weight distribution.

Stereo- and regiodifferentiations obtained from ^{13}C NMR analyses[8] can also be used to estimate activation energy differences. For example, 1% regio errors reflect an energy difference at 70 °C of 3.1 kcal/mol. Halving the number of regiodefects to 0.5% raises the energy difference by 0.5 kcal/mol to 3.6 kcal/mol. Stereodifferentiation is typically reported in terms of the percentage of the polymer with a sequence of five stereoregular insertions or %mmmm.[8,14] Assuming that each insertion event is independent then the fifth root of the mmmm fraction can be used to estimate the stereodifferentiation activation energy difference. Stereoregular pentad distributions of 40%, 90%, and 99% correspond to activation energy differences of 1.1, 2.6, and 4.2 kcal/mol at 70 °C.

Experimental molecular weights and regio- and stereoselectivities can vary substantially from paper to paper for precisely the same catalyst. For example, in 1984 Brintzinger and co-workers[28] and Spaleck and co-workers[29a] reported data for **1** and **2**. Molecular sketches of **1**, **2**, and other catalyst precursors discussed in this review are collected in Figure 1. The Brintzinger group used toluene as the solvent and carried the polymerization out at 50 °C. Spaleck and co-workers carried the polymerization out in liquid

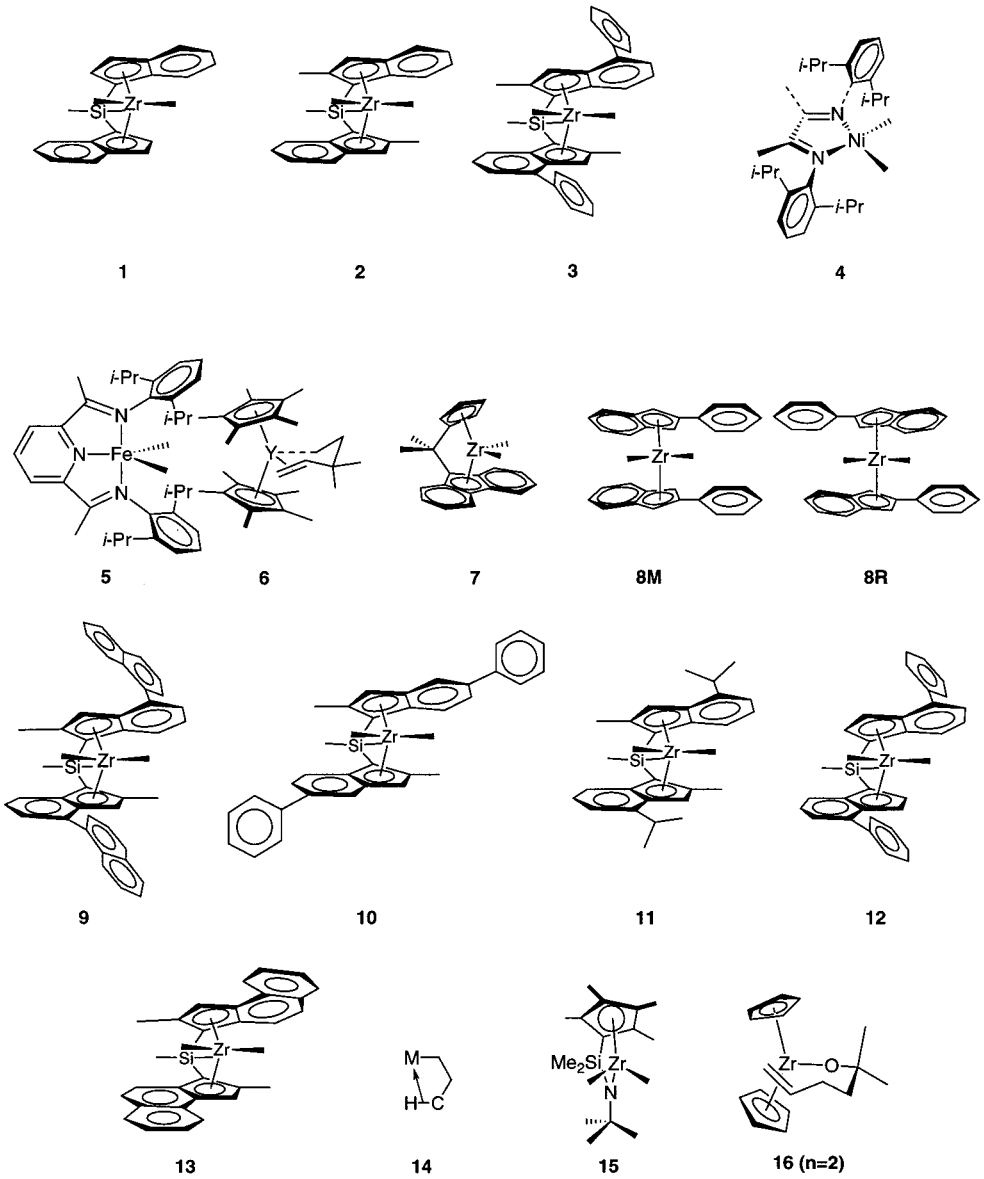

Figure 1. Catalyst precursors and other molecular structures.

propylene at 70 °C. For **1** and **2** the Brintzinger group obtained M_w values of 62 000 and 135 000, whereas Spaleck and co-workers reported M_w values of 36 000 and 195 000 for the same catalyst precursors. Since M_w for **1** dropped while M_w for **2** rose, the differences in experimental conditions did not systematically increase or decrease M_w. For **1** the M_w values correlate with activation energy differences of 5.0 and 4.6 kcal/mol. For **2** the M_w values infer activation energy differences of 5.5 and 5.7 kcal/mol. Both sets of data are consistent with an increase in M_w in going from **1** to **2**, the Brintzinger group data by 0.5 kcal/mol and the Spaleck and co-workers data by a larger 1.1 kcal/mol. Pentad distributions were also reported for **1** and **2**. For **1** and **2** the Brintzinger group obtained %mmmm values of 89 and 90, whereas Spaleck and co-workers reported %mmmm values of 82 and 89. For **1** the %mmmm values correspond to activation energy differences of 2.2 and 2.5 kcal/mol. For **2** the %mmmm values infer activation energy differences of 2.6 and 2.5 kcal/mol. Again, both groups reported an increase in stereoselectivity in going from **1** to **2**, the Brintzinger group data by 0.1 kcal/mol and the Spaleck and co-workers data by 0.3 kcal/mol. In 1994 Spaleck and co-workers reported[29a] a %mmmm for **3** of 95.2; see Figure 1 for the molecular structure of **3**. In 1997 this group reported[29b] the %mm for **3** to be 98.9. The change in stereoselectivity corresponds to a change in activation energy difference estimate of 0.7 kcal/mol (from 3.8 to 3.1 kcal/mol). This anecdotal analysis suggests that small variation in experimental conditions or analysis can impact activation energy differences by on the order of 0.5 kcal/mol. Precise agreement between theory and experiment should not be demanded due to variation in the experimental conditions, but qualitative (±1 kcal/mol) agreement should be achievable.

III. Modeling Methodologies

The active site model of a modern propylene polymerization catalyst,[29] **3**, shown in Figure 2 demonstrates the molecular complexity of the question at hand. A large and elaborate ligand, labeled

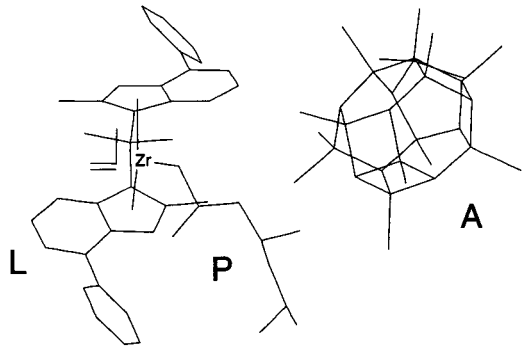

Figure 2. Model active site for olefin polymerization of **3**. **A** denotes the $Al(CH_3)_3{\cdot}Al_9O_9(CH_3)_{10}^-$ counteranion, **P** the polymer chain, and **L** the organic ligand used to achieve stereocontrol and activity enhancement.

L, is required to achieve stereocontrol and the desired polymerization activity. The polymer chain end, labeled **P**, is also known to influence the course of the reaction. The counteranion, labeled **A**, is not an innocent bystander. Despite the large size of this complex, the chain-propagating olefin insertion step only involves two bonds localized on four atoms. Thus, fundamental questions about the electronic structural reorganization accompanying reaction have been answered by computations on compounds containing only a few atoms. However, numerically precise answers to stereocontrol questions likely require hundreds of atoms. The range of modeling methodologies that have been used to study polymerization are described below.

A. Visualization

One cannot underestimate the importance of simple visualization in the catalyst development process. Advances in the stereochemical control of polymerization catalysis have arisen from conceptual models of the 3-dimensional shape of the polymerization active site. For example, the original stereocontrol model of Pino and co-workers[2] started from the crystal structure of the dichloride catalyst precursor. This model is illustrated in Figure 3a. In Pino's active site model, the two chlorides of the crystal structure were removed and a propylene and ethyl chain visually added. The methyl group of the propylene was placed in quadrant Q2. Quadrants Q-1 and Q-2 were excluded "...because of the presence of the $-CH_2-CH_2-$ bridge of the ligand". Q1 was eliminated from consideration because the growing polymer chain occupied it. This model successfully explained the stereochemistry of hydrooligomerization. This work was based on previous models of heterogeneous Ziegler−Natta polymerization.

In general, stereochemical models have been extrapolated from crystal structures of catalyst precursors, usually formulated in the chemist's mind on the basis of observation and intuition, and then sketched with pencil and paper. Experiments were then designed to test the model, and the model was refined in light of the new experiments. Simply "seeing" the active site and iteratively adding steric encumbrances to achieve a desired effect have been enough to advance the field for nearly two decades.[5,28−31]

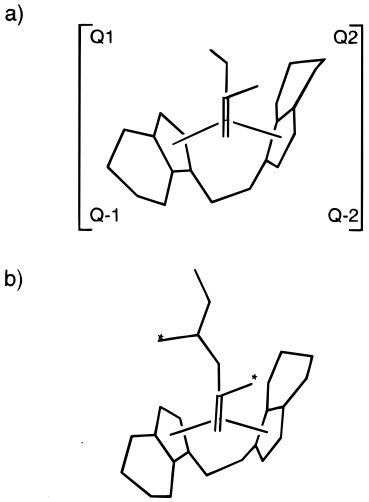

Figure 3. (a) Pino's four-quadrant stereoselectivity model. (b) Corradini's molecular mechanics-based enhancement of the Pino model. The asterisks denote the two methyl groups that control stereoselectivity through steric repulsions.

B. Molecular Mechanics

The next step up from simple visualization is the use of molecular mechanics or force field techniques.[32] Molecular mechanics is a simple computational molecular model that is primarily used for understanding conformational energy differences and structural deviations due to steric interactions in isolated molecules. It also is useful for understanding the nonbonded interactions between molecules. Because bonded atoms are typically held together by unphysical harmonic potentials, the bond-breaking−bond-making events of chemical reactivity are not the natural arena of molecular mechanics. Since the late 1980s the stereochemical and regiochemical differentiation questions of single-center propylene polymerization have been cast as conformational questions—albeit of somewhat distorted structures. Early, useful efforts relied on rigid transition-state models employing variation of only a few torsional degrees of freedom to relieve steric repulsions. This technique had previously been used to understand heterogeneous polymerization. Corradini and co-workers[3] used such a model to confirm Pino's active site model and enhance it to include the impact of the stereochemistry of the growing polymer chain; see Figure 3b. Using molecular mechanics, Corradini and co-workers found that steric interactions between the starred methyl groups were important to stereocontrol. They suggested that the interaction with the polymer chain caused the propylene methyl group to be placed in Q2 rather than the direct interactions between the propylene methyl group and the active site. The active site was proposed to cause the polymer chain to adopt a conformation that led to the chain−monomer repulsion. In 1991 this hypothesis received experimental support from Erker and co-workers' observation[33] of double stereodifferentiation: both enantiomorphic-site control and chain-end control were found to contribute to stereodifferentation.

More recent molecular mechanics studies[34−37] have permitted more complete geometric relaxation to

release steric strain and moderate the magnitudes of the steric effects. Quite recently, full saddle point relaxation has been achieved, and stereo- and regiodifferentiation events comparable in magnitude to experiment have been computed.[38]

C. Electronic Structure

Modern electronic structure technologies do not rely on any knowledge of molecular structure or preconceived ideas about bonding.[39] The geometry of unknown as well as known complexes can be determined. Electronic structure methods can be straightforwardly used to study new compositions of matter and hence novel catalysts. They can also be employed to characterize the transition states of chemical transformations. This freedom comes at the expense of an increased computational effort and a decrease in timeliness, which in the past has largely relegated electronic structure work to a supporting role in understanding polymerization catalysis.

There are signs that the timeliness gap is closing. The first ab initio electronic structure study[40] of a cationic metallocene polymerization catalyst was published in 1989, more than 30 years after its experimental observation in 1957.[41] Molecular modeling studies on stereocontrol by a cationic metallocene polymerization catalyst began to appear in 1988,[3] lagging the experimental report[42] of stereocontrolled polymerization by six years, but following Pino's visualization-based active site model[2] by less than a year. An ab initio electronic structure description of stereocontrol has yet to appear. The first experimental report[6] of a new class of nickel and palladium ethylene catalysts, **4** (see Figure 1), appeared in 1995; ab initio electronic structure studies were published in 1997.[43,44] Novel iron and cobalt ethylene polymerization catalysts, **5** (see Figure 1), were described[45] in 1998, and ab initio electronic structure studies appeared within a year.[46,47]

D. Combined Methods

The time demands of modern electronic structure techniques have limited workers to electronic structure studies on small model complexes. Unfortunately, a number of interesting/important questions in single-center polymerization concern the large steric encumbrances that chemists have added to achieve molecular control. To begin to address these important questions, theorists have begun to develop and apply hybrid methods.[48−51] These methods are a combination of electronic structure methodologies and molecular mechanics techniques. In the most widely used QM/MM technique,[48,49] modern electronic structure theory is used for the atoms involved in electronic reorganization and force field methods are used for the steric periphery. For another hybrid technique termed the reaction potential method,[50,51] electronic structure methods and bonding concepts are used to develop the shapes of potential surfaces[50] and quantum mechanical resonance is used to couple potential surfaces together to describe reactions.[51] Recent theoretical reports highlight the dramatic role that the "real" ligands play.[46,47,52−54]

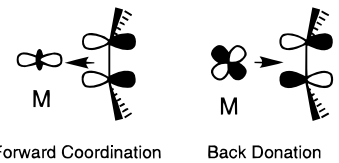

Figure 4. Classic Dewar−Chatt−Duncanson model of metal−olefin bonding.

IV. Olefin Complexation

From the earliest days of metal-catalyzed olefin polymerization, the olefin complexation step, eq 1, has been thought to be important for catalysis. For Ni(II) and Pd(II) catalysts,[6,11] **4**, the olefin binding event is well precedented with numerous crystal structures of olefin complexes.[55] In fact, the resting state of the catalyst is thought to be an olefin complex.[6,11] The binding for these d^8 complexes is properly explained in the terms of the classic Dewar−Chatt−Duncanson model, Figure 4. In this model, bonding consists of a donation of electron density from the olefin π orbital into an empty σ orbital on the metal (forward coordination), and simultaneous donation from a filled metal $d\pi$ orbital into the empty π^* orbital of the olefin (back-donation).

Interestingly, the more common Ti(IV) and Zr(IV) catalysts have d^0 metal centers. The metal cannot participate in back-bonding. Here the bonding must consist entirely of electrostatics, van der Waals interactions, and charge transfer. The dominant interaction has been found to be charge transfer from the olefin to the metal, the forward coordination event of Figure 4; see, for example, ref 56.

Computed olefin complexation energies for a number of ethylene complexes are collected in Table 1.[43,46,47,61−68] There are clear differences in binding energy as a function of theoretical method; it appears as though the major variation is due to the inclusion of electron correlation. Compare entries 32 and 34 with entries 33 and 35−38. Density functional theory (DFT) and correlated wave function approaches give similar results; compare entry 30 with entries 35−38. Despite the differences in the bonding discussed above, d^0 and d^8 metal centers have remarkably similar computed ethylene binding energies. Zirconocene complexes have binding energies of roughly 27 kcal/mol (entry 30), and nickel diimine and palladium diimine complexes in the range of 28−35 kcal/mol (entries 44−46).

This similarity in theoretical Zr and Ni binding energy is inconsistent with experiment. Metallocene polymerizations have a greater than first-order dependence on olefin concentration[34] whereas Ni and Pd catalysts are zeroth-order in olefin.[6,11] A first-order dependence on olefin implies that the resting state of the catalyst does not have an olefin bound. A zeroth-order dependence on olefin is consistent with the catalyst resting state being an olefin complex. The most commonly invoked explanation for the disagreement between theory and experiment is that $M-CH_3$ complexes are not representative of a growing polymer chain.[43,44,65] It has been reasoned that a longer chain would differentiate between Zr and Ni. However, this explanation is negated by the set of binding

Table 1. π Complexation and Insertion Activation Energies (kcal/mol) and M−C and C−C Distances (Å) for $M-CH_3$ Complexes

	compound	method	energies: π complexation	energies: insertion activation	metric parameters: M−C_α	metric parameters: M−C_β	metric parameters: C_α−C_β	ref
1.	$Cl_2TiCH_3^+ + C_2H_4$	HF	36	11	2.11	2.22	1.41	57
2.	$Cl_2TiCH_3^+ + C_2H_4$	HF	41	14	2.86	2.35	1.35	58
3.	$Cl_2TiCH_3^+ + C_2H_4$	DPUMP2	45	4.3				58
4.	$Cl_2TiCH_3^+ + C_2H_4$	HF	34	12	2.15	2.30	1.38	50
5.	$Cl_2TiCH_3^+ + C_2H_4$	HF	35		2.82	2.42	1.34	62
6.	$Cl_2TiCH_3^+ + C_2H_4$	MP2	35		2.75	2.36	1.35	62
7.	$Cl_2TiCH_3^+ + C_2H_4$	LDF	44		2.59	2.29	1.36	62
8.	$Cl_2TiCH_3^+ + C_2H_4$	NLDF−BP	33		2.74	2.37	1.37	62
9.	$Cl_2TiCH_3^+ + C_2H_4$	B3LYP (MIDI4)	34	8	2.74	2.37	1.37	63
10.	$Cl_2TiCH_3^+ + C_2H_4$	B3LYP (6−31 g*)	38	6	2.74	2.37	1.37	63
11.	$Cl_2TiCH_3^+ + C_2H_4$	MP2 (MIDI4)	34	9	2.74	2.37	1.37	63
12.	$Cl_2TiCH_3^+ + C_2H_4$	CAS (MIDI4)	32	15	2.74	2.37	1.37	63
13.	$Cl_2TiCH_3^+ + C_2H_4$	CASPT2 (MIDI4)	35	7	2.74	2.37	1.37	63
14.	$Cp_2TiCH_3^+ + C_2H_4$	PRDDO		21	2.26	2.28	1.38	40
15.	$Cp_2TiCH_3^+ + C_2H_4$	HF		22				40
16.	$Cp_2TiCH_3^+ + C_2H_4$	MP2	16	10				40
17.	$Cp_2TiCH_3^+ + C_2H_4$	LDA	22					64
18.	$Cp_2TiCH_3^+ + C_2H_4$	NLDA	7					64
19.	$Cp_2ScCH_3 + C_2H_4$	GC_DFT	5	3	2.82	2.77		58
20.	$(SiH_2Cp_2)TiCH_3^+ + C_2H_4$	HF	13	14	2.93	2.81	1.33	60
21.	$(SiH_2Cp_2)TiCH_3^+ + C_2H_4$	MP2	29	1				60
22.	$(SiH_2Cp_2)TiCH_3^+ + C_2H_4$	MP3	21	11				60
23.	$(SiH_2Cp_2)TiCH_3^+ + C_2H_4$	MP4SDQ	28	3				60
24.	$(SiH_2Cp_2)TiCH_3^+ + C_2H_4$	QCISD	22	7				60
25.	$Cl_2ZrCH_3^+ + C_2H_4$	HF	37	22	2.90	2.40	1.36	84
26.	$Cl_2ZrCH_3^+ + C_2H_4$	GVB−CI,pol.	33	24				84
27.	$Cp_2ZrCH_3^+ + C_2H_4$	GC-DFT	23	<1	2.50	2.72	1.35	56
28.	$Cp_2ZrCH_3^+ + C_2H_4$	LDA	29					64
29.	$Cp_2ZrCH_3^+ + C_2H_4$	NLDA	14					64
30.	$(SiH_2Cp_2)ZrCH_3^+ + C_2H_4$	GC-DFT	26	1	2.44	2.68	1.36	56
31.	$(SiH_2CpNH)ZrCH_3^+ + C_2H_4$	GC-DFT	27	6	2.72	2.63	1.33	56
32.	$(SiH_2Cp_2)ZrCH_3^+ + C_2H_4$	HF	19	17	2.97	2.90	1.33	59
33.	$(SiH_2Cp_2)ZrCH_3^+ + C_2H_4$	MP2	34	6				59
34.	$(SiH_2Cp_2)ZrCH_3^+ + C_2H_4$	HF	19	17	2.97	2.90	1.33	60
35.	$(SiH_2Cp_2)ZrCH_3^+ + C_2H_4$	MP2	33	6				60
36.	$(SiH_2Cp_2)ZrCH_3^+ + C_2H_4$	MP3	29	10				60
37.	$(SiH_2Cp_2)ZrCH_3^+ + C_2H_4$	MP4SDQ	30	9				60
38.	$(SiH_2Cp_2)ZrCH_3^+ + C_2H_4$	QCISD	29	9				60
39.	$(SiH_2Cp_2)HfCH_3^+ + C_2H_4$	HF	18	18	2.95	2.89	1.33	60
40.	$(SiH_2Cp_2)HfCH_3^+ + C_2H_4$	MP2	32	7				60
41.	$(SiH_2Cp_2)HfCH_3^+ + C_2H_4$	MP3	29	11				60
42.	$(SiH_2Cp_2)HfCH_3^+ + C_2H_4$	MP4SDQ	28	10				60
43.	$(SiH_2Cp_2)HfCH_3^+ + C_2H_4$	QCISD	28	10				60
44.	$(HN{=}C{-}C{-}NH)NiCH_3^+ + C_2H_4$	B3LYP	28	10	2.19	2.19	1.37	43a
45.	$(HN{=}C{-}C{-}NH)NiCH_3^+ + C_2H_4$	GC-DFT	35	11	2.10	2.17	1.37	44
46.	$(HN{=}C{-}C{-}NH)PdCH_3^+ + C_2H_4$	B3LYP	34	16	2.30	2.36	1.38	43b
47.	$(S(C_6H_4O)_2)TiCH_3^+ + C_2H_4$	B3LYP	21	6	2.62	2.69	1.36	54
48.	$(CH_2(C_6H_4O)_2)TiCH_3^+ + C_2H_4$	B3LYP	27	11	2.69	2.48	1.37	54
49.	$((C_6H_4O)_2)TiCH_3^+ + C_2H_4$	B3LYP	27	11	2.71	2.47	1.37	54
50.	$(S(C_6H_4O)_2)ZrCH_3^+ + C_2H_4$	B3LYP	22	7	3.00	2.63	1.37	54
51.	$(CH_2(C_6H_4O)_2)ZrCH_3^+ + C_2H_4$	B3LYP	25	15	2.78	2.28	1.37	54
52.	$((C_6H_4O)_2)ZrCH_3^+ + C_2H_4$	B3LYP	25	16	2.84	2.73	1.37	54
53.	$(H_2O)ClCrCH_3^+ + C_2H_4$	BPW91	27	9	2.25	2.44	1.38	61
54.	$(H_2O)ClCrCH_3^+ + C_2H_4$	HF	22	21				61
55.	$(H_2O)ClCrCH_3^+ + C_2H_4$	MP2	29	9				61
56.	$(H_2O)ClCrCH_3^+ + C_2H_4$	PCI-80	28	10				61
57.	bis(2,6-diisopropylphenylimino)pyridyl-$FeCH_3^+ + C_2H_4$	DFT	39	3	2.00	2.00	1.41	46
58.	bis(imino)pyridyl-$FeCH_3^+ + C_2H_4$	GC-DFT	30	7				47
59.	bis(2,6-diisopropylphenylimino)pyridyl-$FeCH_3^+ + C_2H_4$	CG-DFT	8	0.3				47

energies for more representative $M-C_3H_7$ complexes collected in Table 2.[43,44,65] There is a ~15 kcal/mol drop in ethylene binding energy due to a disruption in β or γ agostic interaction on olefin complexation (see refs 66 and 67 as well as section VII.A for a discussion of agostic interactions). Nonetheless, d^0 and d^8 metal complexes still have similar theoretical olefin binding energies!

Another explanation for the inability to reproduce the experimental observations is that modern electronic structure theory of any flavor as practiced today simply cannot reproduce experimental olefin binding energies. We are not comfortable with this explanation and find support for modern electronic

Table 2. Ethylene Complexation and Insertion Activation Energies (kcal/mol) for M−C_3H_7 Complexes

			energies		
	compound	method	π complexation	insertion activation	ref
1.	(HN=C−C−NH)$NiC_3H_7^+ + C_2H_4$	B3LYP	12	11	43a
2.	(HN=C−C−NH)$NiC_3H_7^+ + C_2H_4$	GC-DFT	19	17	44
3.	(HN=C−C−NH)$PdC_3H_7^+ + C_2H_4$	B3LYP	17	18	43c
4.	(HNCH2CH2CH2NH)$TiC_3H_7^+ + C_2H_4$	GC-DFT	19	8	61
5.	(HNCH2CH2CH2NH)$ZrC_3H_7^+ + C_2H_4$	GC-DFT	22	7	61
6.	(HNCH2CH2CH2NH)$HfC_3H_7^+ + C_2H_4$	GC-DFT	21	10	61

structure theory from olefin binding studies on group 3, Sc and Y complexes. From reaction path competition studies, Casey, Hallenbeck, Landis, and coworkers[68] suggest that the intramolecular olefin binding energy in **6** (see Figure 1) is experimentally less than 10.4 kcal/mol. Through a conformer population analysis of the NOESY time course they also suggest an olefin−metal structure analogous to those reported in Table 1 for d^0 complexes. As indicated in Table 1, entry 19, Woo and Ziegler[56] have reported a computed scandium−ethylene binding energy of 5 kcal/mol.

As discussed in more detail in section VII.B, we believe the disagreement between theoretical and experimental olefin binding energies is a consequence of counteranion or solvent playing a differential role in d^0 versus d^8 metal complexes. The olefin binding energies in Tables 1 and 2 were for bare gas-phase cationic metal complexes failing to include solvent or counteranion. Addition of a counteranion to the cationic computational model[18] drops the HF ethylene binding energy from roughly 35−40 to ~0 kcal/mol for SiH_2(CpNH)$TiCH_3^+$. The roles of ion pairing, counteranions, and solvent will be discussed in section VII.B.

Both the Ziegler[52] and Morokuma[53] groups have reported that addition of the aryl substituents to a model nickel diimine catalyst decreased the stability of the olefin complex. This decrease in group 10 binding energy further enlarges the inconsistency between group 4 and group 10 computed olefin binding energies. The Morokuma group has also found that the nature of the bridge in titanium and zirconium bisphenoxide catalysts strongly impacts the olefin binding energy.[54]

Griffiths, Britovsek, Gibson, and Gould[46] report a DFT ethylene binding energy of 39 kcal/mol for the recently published iron ethylene polymerization catalyst, **5** (entry 57 in Table 1); see Figure 1 for the molecular structure.[45] Deng, Margl, and Ziegler compute[47] an ethylene binding energy of 30 kcal/mol for a related small model complex (entry 58 in Table 1). Distressingly, Deng, Margl, and Ziegler find that olefin complexation is only 8 kcal/mol downhill for the real system, **5**, computed with a combined QM/MM method! There is a discrepancy of 31 kcal/mol between the QM and QM/MM results! We can only speculate what this discrepancy is due to. The DFT calculation likely suffers from significant basis set superposition error since an STO-3G basis was used for the bulk of the ligand (see section VII.B). This error could result in an overestimation of the binding energy by as much as 15 kcal/mol. Since the QM/MM calculation reported by Ziegler and co-workers used the Amber 95 force field[69a] with its too stiff 6−12 van der Waals represention,[69b] it should underestimate the olefin binding energy, but by more than 15 kcal/mol? Another explanation could be incomplete conformational searching[32] by either or both groups.

V. Chain Propagation

Olefin insertion, illustrated in eq 2, is the central feature of olefin polymerization. It is also one of the most computationally studied organometallic reaction steps. From a theoretical perspective, olefin insertion is remarkable simply because it occurs.[70] The reaction is a four-center 2 + 2 process that should be orbitally forbidden.[71] A metal−carbon σ-bond pair reacts with a carbon−carbon π-bond pair. However, the experimentally observed barriers range between 0 and 15 kcal/mol. This energy range is comparable to the range of barrier heights associated with organic radical processes. For example, the barrier for addition of CH_3 to ethylene is 8 kcal/mol.[72] Polymerization barriers are dramatically lower than those observed for "allowed" processes such as the Diels−Alder cycloaddition[73] or the Cope electrocyclic rearrangement[74] where barriers of 25 and 34 kcal/mol, respectively, are observed. Computational studies on the electronic source of this remarkable reactivity are discussed below in subsection A.

Another remarkable attribute of olefin insertion, also with practical significance, is the degree of stereo- and regiocontrol that can be achieved. Propylene lacks hydrogen-bonding or polarity "hooks" that can be used to achieve selectivity, yet stereo- and regiocontrol greater that 99% has been achieved.[29] Modeling studies on the sources of this control are discussed in subsection B.

A final aspect of olefin insertion that has received theoretical study is monomer control in copolymerization. The single published modeling study on monomer control is discussed in subsection C.

A. Electronic Aspects

Due to the importance of the olefin insertion step, increasingly sophisticated electronic structure studies of this reaction have been carried out for nearly three decades. In 1972, Armstrong, Perkins, and Stewart reported a CNDO study[75] of $TiCl_4$·$Al(CH_3)_3$ + C_2H_4, as a model for heterogeneous Ziegler−Natta polymerization. In 1976 Lauher and Hoffmann[76] presented an extended Hückel (EHT) model reaction coordinate for the reaction of Cp_2MH with C_2H_4. In 1978 Thorn and Hoffmann[77] suggested that the stabilizing influ-

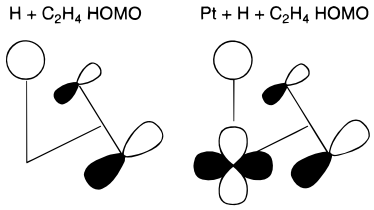

Figure 5. Thorn and Hoffmann molecular orbital description of olefin insertion. The organic radical/anion HOMO is stabilized by a Pt d orbital of proper shape.

ence of a metal d orbital on the H + C_2H_4 HOMO was responsible for the small activation energy associated with olefin insertion for a $L_2Pt(H)(C_2H_4)$ system, Figure 5. That same year Novaro, Blaisten-Barojas, Clementi, Giunchi, and Ruiz-Vizcaya[78] presented a Hartree−Fock (HF) study along a model reaction coordinate for the olefin insertion reaction between $TiCl_4$·$Al(CH_3)_3$ and C_2H_4, again as a model for heterogeneous Ziegler−Natta polymerization. In 1985, Fujimoto and co-workers[79] used an analytic gradient ab initio HF calculation to obtain the saddle point for the reaction of ethylene with $Cl_2TiCH_3^+$ and used interacting molecular orbitals to probe the low barrier found; their explanation was largely in accord with Thorn and Hoffman. At the same time Morokuma and co-workers[80] used an analytic gradient HF calculation to obtain the saddle point for the reaction of ethylene with $Pd(PH_3)(H)_2$. They stressed the importance of agostic interactions in controlling the barrier for the overall reaction. In 1989, Jolly and Marynick[40] used a combination of the approximate partial retention of differential diatomic overlap (PRDDO) method and a HF wave function to characterize the transition state for olefin insertion for both $Cl_2TiCH_3^+ + C_2H_4$ and $Cp_2TiCH_3^+ + C_2H_4$. They found the structures for the Cl and Cp analogues to be quite similar but the energetics for the two systems to be different. In 1992 Morokuma, Koga, and Kawamura-Kuribayashi[81] used a HF calculation to obtain the saddle point for the reaction of ethylene with $Cl_2TiCH_3^+$. The geometries reported were quite similar to the previous results of Fujimoto[79] and Marynick.[40]

In the 1990s a number of HF, second-order Møller−Plesset theory (MP2), and DFT studies have been reported for a host of model catalysts. Since the computed saddle points for insertion are all lower than the energy of the separated reactants, it is not appropriate to term these reaction "barriers" since they do not provide a barrier to the reaction. Instead we will call these energies insertion activation energies. The reported energies, taken relative to the complexed olefin, are collected in Tables 1 and 2. As with the olefin complexation event, addition of electron correlation to the model, through either wave function theory or density functional theory, results in a stable family of insertion activation energies in the range of 5−10 kcal/mol that are, on the surface, consistent with experimental estimates (2−10 kcal/mol).[18] The fact that the computed transition states are energetically below the separated reactants should be of some concern since, as discussed in section IV, all available experimental data are consistent with at least a first-order dependence in olefin for metallacene polymerization.[6] A possible ion-pairing explanation for this anomaly will be discussed in section VII.B.

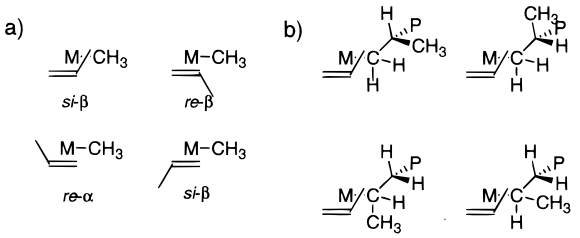

Figure 6. Family of propylene approach possibilities: (a) the four possibilities for a first insertion; (b) four of the sixteen possibilities for additional insertions.

Both the Ziegler[52] and Morokuma[53] groups have reported that addition of the aryl substituents to a model nickel diimine catalyst, **4**, decreased the insertion activation energy by differentially destabilizing the olefin π-complex reactant. The Morokuma group has also found that the nature of the bridge in titanium and zirconium bisphenoxide catalysts strongly impacts the insertion activation energy, again by decreasing the olefin π-complex binding energy.[54]

Griffiths, Britovsek, Gibson, and Gould[46] report an ethylene insertion barrier of 3 kcal/mol for the recently reported iron ethylene polymerization catalyst, **5**.[44] In contrast Deng, Margl, and Ziegler find[47] insertion to not be a facile process for a related small model complex. For **5** they find that the alkyl complex must isomerize prior to insertion, insertion then proceeding with a 0.3 kcal/mol barrier.

B. Stereo- and Regiocontrol

If the olefin being polymerized possesses a substituent, even a substituent as simple as a methyl group (propylene), then the insertion reaction described in eq 2 becomes a family of insertion events. Insertion of an olefin into a metal-methyl bond yields four possible insertion events; see Figure 6a. Two of the insertion events place the olefin's substituent β to the metal in the product, and two place the substituent α to the metal. The first two insertion events are called 1,2 insertions, and the next two are called 2,1 insertions. The two 1,2 insertions correspond with reaction involving the *si* and *re* olefin faces, respectively. The two 2,1 insertions also result from reaction with alternate *si* and *re* olefin faces.

In the case of a vinyl olefin inserting into a metal−alkyl bond of a larger, substituted alkyl chain, for example, a chain formed as a result of previous insertion events, the family of insertion events is squared; see Figure 6b. In Figure 6b only *si* olefin approach is shown for the four possible previous insertion events. Despite this complexity, a very high degree of regioselectivity has been achieved experimentally.[82] Catalysts have also been developed that produce polymer formed from reaction with the same olefin face, called an isotactic polymer,[7,28,29,31] or that selectively produce polymer formed from the reaction with alternating olefin faces, called a syndiotactic polymer.[4,83] As discussed in other reviews,[8,14] the degree of stereo- and regiocontrol in vinyl olefin

polymerization can be determined by ^{13}C NMR spectroscopy. As discussed in section II, experimentally determined stereo- and regiodifferentiations correspond to transition-state energy differentiations of 2−4 kcal/mol. It is remarkable that a simple functional group such as a methyl can lead to a differentiation as large as 4 kcal/mol. It is also daunting that one needs to develop a molecular basis for a differentiation as small as 2−4 kcal/mol. It is difficult to compute bond energies or excitation energies to within a few kilocalories per mole;[39] it is even more difficult to "see" this magnitude of difference.

Stereocontrol of the polymerization of even a nearly 2-dimensional molecule such as propylene is a 3-dimensional (3-D) design exercise.[14] Chemists have developed 3-D sketches of the polymerization active site: in the 1970s for Ziegler−Natta polymerization and in the 1980s for metallocene polymerization. In 1987 Pino, Cioni, and Wei published[2] a four quadrant active site model of isotactic polymerization stereochemical control, based in part on Corradini and co-workers' model for stereocontrol of heterogeneous Ziegler−Natta polymerization.[24] In 1988 Corradini and co-workers[3] enhanced this visualization-based model to include the stereochemical attributes of the isotactic polymer chain. Unfortunately, the computed magnitude of stereodifferentiation was significantly larger than that experimentally observed. Although the computational model explained the experimental observations, it could not be used to predict small or subtle catalyst enhancements.

Despite the importance of understanding regio- and stereocontrol, there have been virtually no electronic structure reports on stereoregular catalyst models. A rare one is provided in a 1992 paper by Morokuma, Koga, and Kawamura-Kuribayashi.[81] A HF wave function was used to obtain the saddle point for the reaction of ethylene with $Cl_2TiCH_3^+$. To investigate the impact of the methyl group of propylene. the authors replaced one of the hydrogens of the ethylene by a standard methyl group. Further geometry optimization was not carried out. With this model they found that the 1,2 or regioregular saddle point was 3 kcal/mol lower than the 2,1 regiodefect saddle point. The first electronic structure study to examine stereoselectivity has just appeared.[14]

In the 1990s, molecular mechanics investigations of stereoselectivity were reported by Castonguay and Rappé,[84] Hart and Rappé,[85] Guerra and co-workers,[37] and Yu and Chien.[34] Here the theoretically derived stereodifferentiation magnitudes were more in line with experiment. In this same time period Kawamura-Kuribayashi, Koga, and Morokuma published[86] a combined ab initio−molecular mechanics study that radically overestimated the energetic differentiation. Here regiodifferentiation greater than 20 kcal/mol was computed for catalysts with experimentally observed regiodifferentiation of at most a few kilocalories per mole. More refined further work from the Morokuma group[85] dropped the regiodifferentiation energies to ∼10 kcal/mol, though the computed stereodifferentiation rose to 16 kcal/mol for a catalyst with an experimentally observed stereodifferentiation of roughly 4 kcal/mol.[29]

In general, the original Pino−Corradini model has worked well, providing a framework for catalyst development.[7,28−31] Recent theoretical studies have gone beyond understanding the stereocontrol of isotactic polymerization to include the control of syndiotactic polymerization,[83] subtle activity questions,[29] and the generation of block homopolymers.[30] This recent work is summarized below and reviewed in detail elsewhere.[14]

The model for syndiotactic polymerization is a bit more complex than the model needed for isotactic polymerization. In 1988 Ewen and co-workers[83] reported the discovery of a metallocene catalyst, isopropyl(cyclopentadienyl-1-fluorenyl)zirconium dichloride, **7**, that would produce syndiotactic polypropylene, that is, a polymer formed from the sequential reaction of alternate olefin π-faces (see Figure 1 for the molecular structure). In contrast to the family of catalysts that have C_2-symmetric catalyst precursors, **7** is C_s-symmetric. Ewen proposed that, for this catalyst to produce syndiotactic polymer, the active site must isomerize after each insertion consistent with the polymer chain flipping from one side to the other during insertion. Stereoerrors were thought to be due to chain "back-skipping" or reaction with the wrong olefin face. For C_2 symmetric catalyst precursors, the active site does not isomerize if the polymer chain flips from side to side.

In 1991 Guerra and co-workers[88] reported a few-degrees-of-freedom force field study on metallocene syndiotactic polymerization. Their modeling work supported Ewen's proposal and suggested again that the polymer chain was the primary source of stereocontrol. The catalyst active site shape was responsible for providing the preferred orientation for the polymer chain. In contrast to the isospecific C_2-symmetric active sites where the chain and propylene each can be placed in a steric "hole", here the steric demands of the chain induce the propylene methyl group to be pointed toward the more substituted fluorenyl ring.

The suggestion that the polymer chain flips from one active site side to the other side during insertion and then stays there until the next insertion event prompted several computational efforts. Starting with the work of Jolly and Marynick,[89] most theoretical studies have found that group 14 metallocenium ions are pyramidal at the metal center. Bierwagen, Goddard, and Bercaw explained[90] the pyramidal nature of the metal center in terms of %d character in the M−X bonds; cationic complexes were found to possess bonds with a higher %d character and lower %s character in the metal orbitals that contributed to the M−X bonds. Since X−M−X bond angles assembled from bonds involving d orbitals are smaller than those comprising s orbitals,[91] Bierwagen, Goddard, and Bercaw explained that a larger %d character corresponded to a greater degree of pyramidalization. Further, computed barriers to inversion at the metal or back-skipping were found to be quite small; see Table 3. The computed barriers in Table 3 are not consistent with retention of active site stereochemistry. Theory predicts that the active site

Table 3. Computed Inversion Barriers (kcal/mol)

	compound	method	inversion barrier	ref
1.	$Cl_2TiCH_3^+$	HF	3	89
2.	$Cl_2TiCH_3^+$	GVB−CI	8	90
3.	$Cp_2TiCH_3^+$	GVB−CI	−4	90
4.	$Cl_2ZrCH_3^+$	HF	4	84

should randomize between insertion events. In addition to being inconsistent with experimentally observed polymerization stereochemistry, the computed barriers to inversion are in conflict with Yang, Stern, and Marks' report[92] of an experimental 18 kcal/mol barrier for the reaction shown in eq 6. To

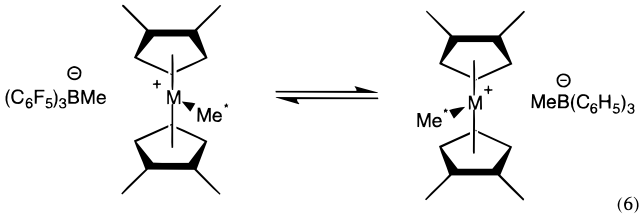

(6)

understand this discrepancy, Castonguay and Rappé[84] carried out a modeling study on the reaction in eq 6 which explicitly included the borate counteranion; an increase in inversion barrier resulted (the barrier rose from 3 to 10−11 kcal/mol). Further discussion of counteranion modeling is presented in section VII. B. Alternative explanations for the observed stereocontrol include agostic stabilization and solvent stabilization of the alkyl intermediate.

In addition to contributing to our understanding of stereocontrol, modeling has been used to probe the sources of regiocontrol. In 1997 Guerra and co-workers compared[37] the regioselectivity of catalysts which make isotactic polymer with catalysts which make syndiotactic polymer. In agreement with experiment, they found that both catalyst families were self-correcting; that is, chain ends resulting from regiodefect insertions preferentially reacted with the propylene orientation that would return to proper chain growth. In contrast to normal chain growth where the stereocontrol was dominated by interactions with the chain end, Guerra and co-workers attributed regiodefect stereocontrol to the metal−ligand active site.

In 1995 Coates and Waymouth[30] reported a catalyst that produced polypropylene-containing blocks of atactic polypropylene and isotactic polypropylene. This novel elastomeric material was referred to as elastomeric homopolypropylene (EHPP). The unit cell of the crystal structure of the EHPP catalyst precursor bis(2-phenylindenyl)zirconium dichloride was observed to contain two distinct conformers; see Figure 1 for the structures. In one conformer, **8M**, the indenyl ligands were *syn* to one another (a *meso* stereochemistry), while in the other conformer, **8R**, the indenyl ligands were *anti* to one another (a *rac* stereochemistry). Production of isotactic blocks of polypropylene could be explained by polymerization from the *rac* active site and production of atactic blocks by polymerization from the *meso* active site. In 1996 Pietsch and Rappé published[93] a molecular mechanics study suggesting that switching between the *rac* and *meso* active site shapes was controlled by π-stacking interactions between the phenyl substituents in the *rac* conformer and between phenyl rings and the benzo groups of the indenyls in the *meso* conformer. This π-stacking model and underlying force field technology have been used at BP-Amoco as an important part of the EHPP catalyst development effort.[94]

Table 4. Summary of Substituted Indenyl Catalyst Precursor Data[a]

catalyst	polymer yield (g)	productivity [kg of PP/(mmol of Zr h)]	M_w ($\times 10^{-3}$)	mp (°C)	mmmm (%)
1	956	190	36	137	81.7
2	492	99	195	145	88.5
3	2640	755	729	157	95.2
7	2620	875	920	161	99.1
8	314	63	188	139	78.1
9		245	213		88.6
10	240	48	42	148	86.5

[a] From ref 29. Reactions carried out in liquid propylene at 70 °C with a Zr:Al ratio of 1:15000.

One of the major branch points in the single-center catalyst evolution was reported in 1994 by Spaleck and co-workers.[29] They found that by appropriate ligand modification of **1** they were able to achieve enhanced stereocontrol, increased molecular weight, and improved catalyst productivity. A portion of the Hoechst data are collected in Table 4. Placement of a methyl substituent in the 2 position of the indenyl rings of **1** leading to **2**, when coupled with the addition of phenyl or naphthyl substituents in the 4 positions of the indenyl rings (**3** and **9**), led to improved performance in productivity, molecular weight, and stereoselectivity. Placement of the aromatic substituent in the 5 position, **10,** rather than the 4 position, provided no beneficial effect. Placing an isopropyl group in the 4 position, **11**, ruled out a simple steric effect. Removing the methyl group from position 2, **12**, also eliminated the enhancement. In an adjoining paper in *Organometallics*, Brintzinger and co-workers[28] reported an analogous benzo-substituted indenyl catalyst, **13**, which also did not display the remarkable attributes of **3** and **9**. Simple electron donation by an aromatic ring could not be the explanation.

The observations summarized in Table 4 are exciting. Normally, attempts to improve catalyst performance result in a tradeoff between increasing activity and increasing selectivity; adding large groups to control the reaction also slows the reaction. To understand the source of the remarkable influence of the 4 position substituent, Bormann-Rochotte and Rappé carried out a reactive force field[50,51] study[38] of the various pathways for chain propagation for **9**. Briefly, they found enhanced stereoselectivity and regioselectivity for **9** over **1**. Both stereo- and regiodefect sites were found to be self-correcting; that is, the barriers for returning to normal chain growth were found to be lower than barriers to continue defect growth just as reported by Guerra and co-workers.[37] In contrast to Guerra and co-workers' study, Bormann-Rochotte and Rappé found that the

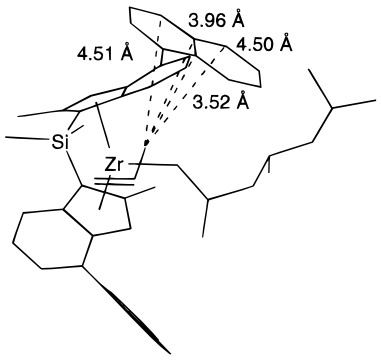

Figure 7. Attractive van der Waals interactions between the methyl group of the approaching propylene and one of the aryl rings of **7**.

polymer chain played a significant role in the stereo- and regiocontrol of the defect chains. Relative barrier heights for propagation and termination steps with (catalyst **9**) and without (catalyst **1**) the 2 position methyl and 4 position naphthyl substituent were found to be consistent with increased molecular weight and increased productivity. Addition of the naphthyl substituent decreased the stereoregular insertion barrier by 1.4 kcal/mol and raised the β-hydride termination by 3.5 kcal/mol.

The most intriguing computational observation was the decrease in insertion barrier caused by the addition of the naphthyl substituent. Addition of a steric encumbrance decreased the barrier! Visual examination of the insertion saddle point provided an explanation for this observation; see Figure 7. At the insertion saddle point the methyl group of the propylene was found to be within van der Waals contact of the aromatic ring and placed in the attractive well of the interaction rather than the inner repulsive wall. In the reactants this stabilizing van der Waals interaction was absent; thus, the saddle point was differentially stabilized.

C. Monomer Control

A major distinction between heterogeneous Ziegler−Natta polymerization and single-center polymerization is the facility with which comonomers are incorporated into the chain.[7] Adding steric encumbrances to the catalyst has been shown to enhance this effect. With the parent biscyclopentadienylzirconocene dichloride, ethylene polymerizes 25 times faster than propylene, with the ethylene tetrahydroindenyl complex ethylene is polymerized 10 times faster than propylene,[31] and with the 2-methyl-4-aryl complexes such as **3** or **9**, ethylene and propylene are polymerized with comparable rates.[29]

In 1997 Schneider, Suhm, Mülhaupt, Prosenc, and Brintzinger reported[95] that benzannelation, **13**, enhances the incorporation of octene in an ethylene−octene copolymerization. To explain this remarkable observation, they carried out a molecular mechanics study and indeed found that **13** has a smaller transition-state energy difference between ethylene insertion and octene insertion than the parent complex **1**.

VI. Chain Termination Steps

Olefin insertion has been observed for complexes of nearly every transition metal and most lanthinides and actinides as well, the notable exception being group 17 metals.[13] As discussed in section V.A, low insertion barriers have been computed for most classes of catalytically active complexes as well. One might speculate that any metal alkyl complex with the potential for a vacant coordination site would make polymer. This expectation is not experimentally realized because chain termination pathways compete with propagation. These termination pathways can be activated by a number of factors. Polymerization catalysts can be converted to oligomerization or dimerization catalysts simply by changes in the solvent or counteranion. The commonly proposed termination pathways are discussed below.

A. β-Hydride Elimination

The classic chain termination pathway is simply the microscopic reverse of olefin insertion; see eq 3. If a hydrogen is transferred to the metal, the reaction is called a β-hydride elimination. If a methyl is transferred to the metal, the reaction is called a β-methyl elimination. β-Methyl elimination has been documented for lanthinides by Watson[95] and for zirconocenes by Resconi.[96] Given the generally accepted electronic explanation for the low barriers for olefin insertion,[70,76−81] one should also expect low barriers for the hydrogen insertion reaction and its complementary β-hydride elimination pathway. The major hurdle for the elimination pathways is thermodynamics. Olefin insertion events are exothermic, ~22 kcal/mol per ethylene unit measured from free ethylene.[97] The microscopic reverse β-methyl elimination event is endothermic by a comparable amount. This thermodynamic analysis ignores the olefin complexation energy that can stabilize the eliminated product. Given that a hydrogen is smaller than a polymer chain or even a methyl group, olefin complexation energies for metal hydrides are ~10 kcal/mol larger than for metal methyl complexes; compare Tables 1 and 5. Computed β-hydride and β-methyl elimination barriers are also collected in Table 5. Hydride and methyl elimination events are computed to be competitive. Hydrogen insertion is computed to have a smaller barrier than methyl insertion.

The energy difference between β-hydride elimination termination and ethylene propagation is in reasonable accord with experimentally determined molecular weights. For example, the QCISD insertion activation energy for $(SiH_2Cp_2)ZrCH_3^+$ has been reported[61] to be 9 kcal/mol and the β-hydride elimination activation energy, 14 kcal/mol. This corresponds to a molecular weight of roughly 100 000.

B. β-Hydride Transfer to Monomer

In addition to β elimination, Brintzinger and coworkers[28] have suggested chain termination occurs through a direct transfer of a β hydrogen to an incoming monomer; see eq 4. Transfer to monomer and β-hydride elimination pathways can, in principle, be differentiated by their dependencies on monomer

Table 5. Metal−Hydride Propylene Complexation, Hydrogen Insertion Activation, β-Hydride Elimination Activation, and β-Methyl Elimination Energies (kcal/mol)

		energies				
compound	method	π complexation	insertion activation	β-H elimination	β-Me elimination	ref
$(SiH_2Cp_2)TiH^+ + C_3H_6$	HF	24	1	19	28	60
$(SiH_2Cp_2)TiH^+ + C_3H_6$	MP2	41	2	19	16	60
$(SiH_2Cp_2)TiH^+ + C_3H_6$	MP3	33	0	20	27	60
$(SiH_2Cp_2)TiH^+ + C_3H_6$	MP4SDQ	39	1	18	15	60
$(SiH_2Cp_2)TiH^+ + C_3H_6$	QCISD	34	0	18	21	60
$(SiH_2Cp_2)ZrH^+ + C_3H_6$	HF	26	6	16	24	60
$(SiH_2Cp_2)ZrH^+ + C_3H_6$	MP2	39	1	14	14	60
$(SiH_2Cp_2)ZrH^+ + C_3H_6$	MP3	35	3	15	17	60
$(SiH_2Cp_2)ZrH^+ + C_3H_6$	MP4SDQ	36	3	14	16	60
$(SiH_2Cp_2)ZrH^+ + C_3H_6$	QCISD	35	3	14	16	60
$(SiH_2Cp_2)HfH^+ + C_3H_6$	HF	26	6	17	26	60
$(SiH_2Cp_2)HfH^+ + C_3H_6$	MP2	42	2	15	15	60
$(SiH_2Cp_2)HfH^+ + C_3H_6$	MP3	38	3	16	18	60
$(SiH_2Cp_2)HfH^+ + C_3H_6$	MP4SDQ	38	3	15	17	60
$(SiH_2Cp_2)HfH^+ + C_3H_6$	QCISD	37	3	15	17	60
$(HN{=}C{-}C{-}NH)NiH^+ + C_3H_6$	B3LYP	39	<1	14	21	43a
$(HN{=}C{-}C{-}NH)PdH^+ + C_3H_6$	B3LYP	44	<1	5	10	43b

Table 6. Ethylene Complexation, Ethyl Insertion Activation, β-Hydrogen Transfer to Monomer Activation, β-Hydride Elimination Activation, and Hydrogen Insertion Activation Energies (kcal/mol)[a]

		energies				
	compound	π complexation	ethyl insertion activation	β-H transfer to monomer	β-H elimination	β-Me insertion activation
1.	Cp_2ScR	1	1	9	15	0
2.	Cp_2TiR^+	3	4	8	34	0
3.	Cp_2ZrR^+	11	4	7	11	1
4.	Cp_2HfR^+	15	4	9	10	3
5.	$(SiH_2CpNH)TiR^+$	18	5	7	15	2
6.	$SiPh_2CpFluZrR^+$				10	4

[a] From ref 99b,c. Ethylene complexation, ethyl insertion activation, and β-hydrogen transfer to monomer activation energies were obtained for ethylene−ethyl complexes.

concentration. β-Hydride elimination should be independent of olefin concentration, whereas transfer to monomer should be linearly dependent upon olefin concentration. Since propagation is dependent on olefin concentration for d^0 catalysts, and the molecular weight for a Shultz−Flory distribution is proportional to the ratio of propagation to termination rates, the dependence of molecular weight on olefin concentration should be a measure of termination pathway. In 1994 Brintzinger and co-workers reported[28] that **13** produced polymer with a molecular weight independent of monomer concentration, consistent with termination through transfer to monomer (eq 4). For this scenario both propagation and termination rates would be dependent upon monomer concentration, and monomer concentration dependence would cancel out. Addition of methyls to the 2 position of the indenyl rings generated a catalyst that produced polymer with a molecular weight strongly dependent on monomer concentration, consistent with termination via β-hydride transfer. Here, since β-hydride transfer termination is independent of monomer concentration, the relative rates of propagation and termination, and hence molecular weight, would be strongly dependent upon monomer concentration.

To explain this methyl group pathway differentiation, Brintzinger and co-workers[28] presented the first model for transfer to monomer and suggested that 2-methyl substitution on the indenyl effectively blocked the transfer to monomer pathway. This pathway, eq 4, has received scattered theoretical attention; prior to the 1999 report by Margl, Deng, and Ziegler[99b,c] only a few transfer to monomer barriers had been reported. Lohrenz, Woo, Fan, and Ziegler calculated a barrier of 7 kcal/mol for $Cp_2ZrC_2H_5$ plus ethylene.[99a] For a small nickel model of **4** Deng, Margl, and Ziegler computed a barrier of 10 kcal/mol. A portion of the recent Margl, Deng, and Ziegler data are collected in Table 6. The transfer to monomer termination pathway is found to be preferred over β-hydride elimination in general. The energy differences between transfer to monomer and insertion in Table 6 are too small to be consistent with polymer formation; however, the precise molecules of Table 6 are not good polymerization catalysts.

In 1996 Cavallo and Guerra reported[35] a combined DFT/molecular mechanics study addressing the termination pathway differentiation discussed above that was observed by Brintzinger and co-workers.[28] Saddle points for β-hydride transfer and β-hydrogen transfer to monomer termination steps were obtained for $Cp_2ZrC_2H_5^+$ and $Cp_2ZrC_4H_9^+$, respectively. The β-hydride transfer to metal pathway was calculated to be too high in energy to be a viable termination pathway. The β-hydrogen transfer to monomer termination pathway was found to be 7 kcal/mol above

the insertion pathway. This result suggests that Cp_2ZrCl_2 should make polymer with a molecular weight greater than 100 000 at 70 °C. Experimentally molecular weights of 200−1000 are observed for Cp_2ZrCl_2.[7] Next Cavallo and Guerra extended the polymer chain and replaced the Cp's by either benzoindenyl or 2-methyl benzoindenyl ligands. The essential saddle point features of the DFT model were fixed for the molecular mechanics work. In going from an ethylene−ethyl model to a propylene−pentyl chain model, the transfer to monomer transition state was differentially raised, leading to a prediction of even longer chains. Cavallo and Guerra also studied the impact of the 2-Me substituent on a benozindenyl catalyst model. The 2-Me group was found to raise the insertion transition state by 3 kcal/mol. Experimentally, addition of a 2-Me substituent is observed to decrease catalyst productivity by a factor of 2−4, which corresponds to an activation energy perturbation of 0.4−0.9 kcal/mol. The β-hydride transfer to metal termination pathway was computed to be unaffected by the presence of the 2-Me substituent. The β-hydrogen transfer to monomer termination pathway was calculated to be differentially raised, relative to the β-hydride transfer to metal pathway, by 1.3 kcal/mol. If the β-hydride transfer to metal termination pathway had been computed to be competitive with β-hydrogen transfer to monomer for the parent Cp_2ZrCl_2 system, then a 1.3 kcal/mol pathway bias could have been enough to explain the experimentally observed pathway differentiation. As it is, the trend is in the correct direction, but does not explain a termination pathway switch. It should be noted that in section VII.D we describe the work of Prosenc and Brintzinger[100] wherein they find a DFT β-hydride transfer to metal barrier of only 10 kcal/mol for an isobutyl chain. If Cavallo and Guerra had computed this magnitude for the β-hydride transfer to metal termination barrier, their results would have been in agreement with experiment.

Both the Ziegler[52] and Morokuma[53] groups have reported that addition of the aryl substituents to a model nickel diimine catalyst, **4**, increased the transfer to monomer barrier by destabilizing the axial site needed for olefin approach.

Deng, Margl, and Ziegler[47] find transfer to monomer to be quite competitive with insertion for the recently reported iron ethylene polymerization catalyst, **5**.[45] The highest points on the propagation and transfer to monomer pathways differed by only 0.8 kcal/mol, not a good way to make polymers.

C. Chain Transfer to Counteranion

Another experimentally observed termination pathway is transfer of the growing polymer chain to the counteranion, eq 5.[45] Unfortunately, there have not been any computational studies of this pathway.

VII. Other Issues

During the course of developing a mechanistic understanding of single-center polymerization, a number of physical organic tools have been employed. These include studies on model systems,[101−103] isotopic labeling experiments,[101−104] and probes of ion pairing or specific ion effects.[12,16,92,105−109] Computational studies in support of these physical organic efforts are summarized here.

A. Agostic Effects

The original Cossee−Arlman mechanism for Ziegler−Natta olefin polymerization has withstood more than three decades of active research and several alternative suggestions for the reaction pathway. Recent developments suggest that a "modified Green−Rooney mechanism" wherein α-agostic interactions as proposed by Green and Brookhart[66] might be necessary to explain the subtleties of single-center polymerization and lead to advances in the development of new stereoregular polymerization catalysts. In general, electrophilic or coordinatively unsaturated transition-metal complexes are observed to form unusually short C−H nonbonded contacts; see **14**, Figure 1. The interactions associated with these contacts are thought to stabilize the metal center. In addition to decreasing nonbonded M−H distances, agostic interactions lengthen the associated C−H bond and decrease the C−H stretching frequency.[66] Grubbs and co-workers[101] reasoned that if α-agostic interactions are present in the transition state for olefin insertion then a secondary kinetic isotope effect should be observed if hydrogen is substituted by deuterium.

The specific reactions studied by Grubbs and co-workers,[101] eq 7, Piers and Bercaw,[102] eq 8, and Krauledat and Brintzinger,[103] eq 9, are closely related

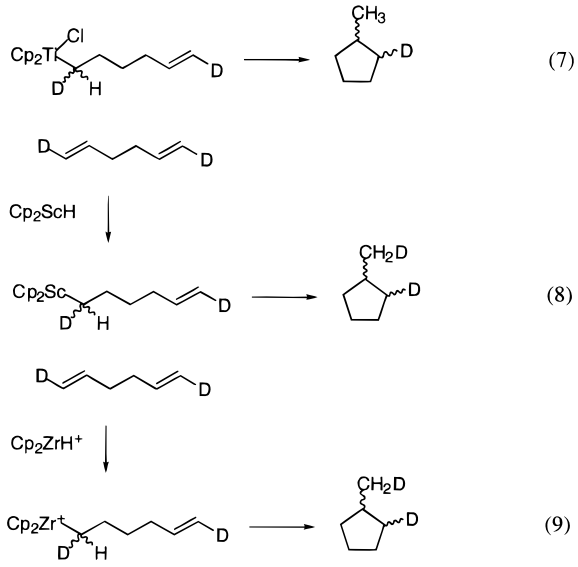

and point out the delicate energetic balance associated with agostic interactions and the differentiation in the precise orientation of the growing polymer chain for different catalysts. A kinetic isotope effect of 1.26 was observed for eq 8, suggesting an α agostic interaction. Kinetic isotope effects were not observed for eqs 7 and 9, suggesting that differential α agostic interactions were not present. In the related Cp_2ZrCl_2/MAO-catalyzed hydrodimerization of 1-deuterio-1-hexene, Krauledet and Brintzinger[103] observed a kinetic isotope effect of 1.3.

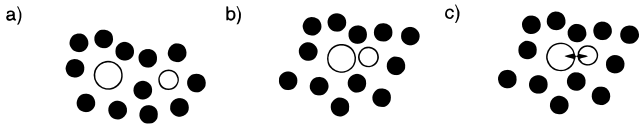

Figure 8. (a) Solvent-separated ion pair model. (b) Contact ion pair model. (c) Resonance-stabilized ion pair model.

Leclerc and Brintzinger[104] observed a kinetic isotope effect in a competition study between (*E*)- and (*Z*)-[D_1]propene. Perhaps more startling they observed the polymer chain to epimerize; see eq 14. The methyl side chains were also found to incorporate a single deuterium. Computational studies of this chain isomerization are discussed in section VII.D below.

In 1992 Prosenc, Janiak, and Brintzinger[110] published an extended Hückel study of the importance of agostic interactions in stereoselective olefin polymerization. They found that Zr−H(α) interactions are net repulsive in the reactant π complex, attractive in an eclipsed transition state, and consistent with a kinetic isotope effect of 1.25. They further found a significantly attractive γ agostic interaction in the propyl product and suggested this interaction was due to the strongly electron deficient nature of the zirconocene cation. They also suggested that this strong interaction could be diminished by an external ligand species.

To understand the differences among the Grubbs, Bercaw, and Brintzinger systems, Wiser and Rappé have computed[111] the secondary kinetic isotope effects for the insertion transition states for each of the reactions of eqs 7−9. A calculated kinetic isotope effect of ∼1.3 was obtained for each insertion transition state. Wiser and Rappé suggested that the lack of a kinetic isotope effect in the Grubbs system was due to an alternative rate-limiting step for this reaction. The observation and nonobservation of kinetic isotope effects were also explained by Coates and Grubbs[66] in terms of differing rate-determining steps (olefin complexation versus olefin insertion) for the systems.

B. Counteranion Effects

A growing body of literature suggests that while the olefin polymerization active site does consist of a cationic metal alkyl, it is not an isolated cationic site.[12,16,92,105−109] The counteranion is likely present as a solvent-separated or contact ion pair; see parts a and b, respectively, of Figure 8. The mechanism for ion pair formation and the observed crystal structures of a few of these ion pairs also suggest an added degree of complexity.[12]

The commonly accepted mechanism for catalyst activation involves abstraction of a methide ion from a metal methyl complex; see eq 10. Marks and co-

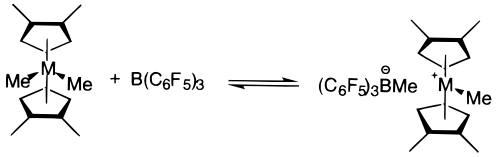

(10)

workers[12,16,92,106] have measured the activation parameters and thermodynamics of this process; a portion of these data are collected in Table 7. Negative values indicate that the reaction in eq 10 is favored in the forward direction. The data are consistent with bond energy expectations (Hf > Zr) and sterics (Me_5Cp > 1,2-Me_2Cp). MAO appears to be a less powerful methide-abstracting agent than $B(C_6F_5)_3$. Given the three-center/two-electron bonding attributes of group 3 and 14 elements and the observation of symmetrically bound methyl groups in group 3 and 14 element compounds, it is not possible to discount a contribution from the neutral resonance structure in the ion pair, eq 11.

Table 7. Experimental Methide Extraction Energetics (kcal/mol)[a]

compound	methide extaction energy
$(1,2\text{-}Me_2Cp)_2Zr(CH_3)_2 + B(C_6F_5)_3$	−24
$(1,2\text{-}Me_2Cp)_2Hf(CH_3)_2 + B(C_6F_5)_3$	−21
$(1,2\text{-}Me_2Cp)_2Zr(CH_3)_2$ + MAO	−11
$(1,2\text{-}Me_2Cp)_2Hf(CH_3)_2$ + MAO	−9
$(Me_5Cp)_2Zr(CH_3)_2 + B(C_6F_5)_3$	−37
$Cp_2Zr(CH_3)_2 + B(C_6F_5)_3$	−23
$(1,2\text{-}Me_2Cp)_2Zr(CH_3)_2 + B(C_6F_5)_3$	−24
$Me_2Si(Me_4Cp)(^tBuN)Ti(CH_3)_2 + B(C_6F_5)_3$	−23
$Me_2Si(Me_4Cp)(^tBuN)Zr(CH_3)_2 + B(C_6F_5)_3$	−24
$Me_2Si(Me_4Cp)(^tBuN)Hf(CH_3)_2 + B(C_6F_5)_3$	−1

[a] From ref 106c.

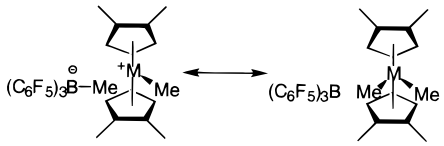

(11)

The contribution of this second resonance structure can be diagnosed structurally. Nonbonded Zr−C close contacts fall in the range of roughly 2.86 Å.[112] Polarcovalent Zr−C distances are typically 2.2−2.3 Å.[113] Observed and computed structures of zirconocene ion pairs place the Zr−C distance at roughly 2.4−2.5 Å.[12] These distances, intermediate between bonded and nonbonded distances, and the observation of coordination of the methyl to the metal for $(C_6F_5)_3BCH_3^-$ rather than coordination through the more donating fluorine provide strong support for an admixture of neutral and ionic resonance structures in zirconocene "contact" ion pairs, eq 11. This suggests the need for another designation for ion pairing; in addition to solvent-separated ion pairing (SSIP) and contact ion pairing (CIP), metallocenium complexes participate in resonance-stabilized ion pairing (RSIP); see Figure 8c.

The contribution of the neutral resonance structure in eq 11 should be proportional to the energy difference between the neutral and ionic forms. The smaller the gap between the ion pair structure and the neutral structure, the shorter the Zr−C "nonbonded" distance should be. From the data in Table 7, MAO−CH_3^- should have a stronger, shorter Zr−C "interaction" than $(C_6F_5)_3BCH_3^-$.

Variable-temperature dynamic NMR studies on a variety of substituted Cp systems by the Marks[12,106] and Siedle[107] groups suggest that CIP or RSIP is the rule rather than the exception in nonpolar solvents

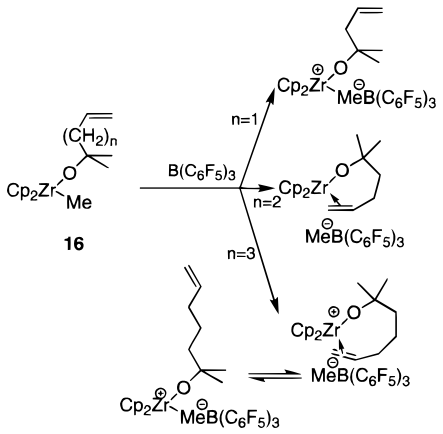

Figure 9. Wu and Jordan olefin−counteranion competition study.

such as toluene and even polar chlorinated solvents such as dichloromethane. The basic experiment monitors the symmetrization of Cp proton resonances that occurs through the equilibration shown in eq 6. The observed free energy barriers for this process range from 14 kcal/mol to greater than 19 kcal/mol depending upon the ligand and counteranion. For [(9-fluorenyl)$_2$C$_2$H$_4$]ZrMe$^+$ the free energy barrier ranges from 14 kcal/mol for MAO−CH$_3^-$ as counteranion to 18 kcal/mol for MeB(C$_6$F$_5$)$_3^-$ as counteranion.[106c]

Perhaps the most striking example of how ion pairing can impact catalysis is found in the monocyclopentadienyl (MCP) or constrained geometry catalyst family, **15**, discovered by Bercaw and coworkers; see Figure 1 for the molecular structure.[114] This system possesses a particularly open active site. In the Exxon extrapolation of the Bercaw Sc catalyst to Ti, Canich reported[115] the production of crystalline poly-α-olefins for several of the substituted Cp systems. That is, poly-α-olefins with enriched isotacticity were produced. In the Dow extrapolation of the Bercaw Sc catalyst to Ti, syndiotactic polymer was produced.[116] Subsequent efforts have reported slightly enhanced syndiotacticity[117] and counteranion-dependent isotacticity.[118] The most obvious difference between the Dow and Exxon reports is the solvent. Aside from differences in the Cp ring substitution, Dow utilized Isopar E as solvent whereas Exxon employed toluene.

Olefin binding and counteranion binding are competitive. This supposition is supported by experimental work from the Jordan lab. As shown in Figure 9 Wu, Jordan, and Petersen[119] find the olefin binding affinities of coordinated vinyl alkoxides to be strongly dependent upon the length of the alkyl chain (*n*). For **16**, $n = 1$, a contact ion pair is formed with the borate salt. For **16**, $n = 2$, the vinyl substituent binds to the metal center, and for **16**, $n = 3$ there is an equilibrium between complexed olefin and contact ion pair forms. This observed competition between ion pair formation and olefin complexation can be taken with the Deck and Marks[106a] measurement of the ion pair dissociation energetics to estimate the olefin binding energies in Jordan's complexes.

Deck and Marks find the experimental free energy for ion pair dissociation to be 19 kcal/mol in toluene and 15 kcal/mol in chlorinated solvents (for the MeB(C$_6$F$_5$)$_3^-$ anion and a set of related zirconocene complexes). Since Jordan's system involves intramolecular olefin binding, the Deck and Marks 15 kcal/mol free energy should correspond roughly to a 15 kcal/mol binding enthalpy. Further, for Jordan's system the ion pair binding energy should be smaller because of the presence of the alkoxy substituent. Since there is an equilibrium between ion pair and olefin-complexed structures for **16**, $n = 3$, the olefin binding energy for **16**, $n = 3$ should be smaller than 15 kcal/mol. Wu, Jordan, and Petersen also observe Cp diastereotopic protons to be equivalenced by a process with a $\Delta G^{\ddagger}$ of 11 kcal/mol. This is also consistent with an olefin binding energy smaller than 15 kcal/mol. Experimental olefin binding energies of 10−15 kcal/mol would be dramatically inconsistent with the computed olefin binding energies reported in Tables 1 and 2.

To see whether modern electronic structure methodologies can reproduce experimental olefin binding energies, we have studied the Wu, Jordan, and Petersen system with a B3LYP density functional approach[120] using a 6-31g* basis.[121] The LANL2 effective core potential and basis were used for Zr.[122] For each complex the geometry was optimized without constraints using G98.[123] The results are collected in Table 8. The experimental structure for **16**, $n = 2$, is well reproduced and the $n = 1$, $n = 2$, and $n = 3$ data follow the experimental energetic trend.[119] We find the $n = 2$ case to be virtually strain-free; the binding energy for the $n = 2$ ring system, 18 kcal/mol, is 1 kcal/mol more than that of the analogous ethylene complex. Our Cp$_2$Zr−CH$_3^+$ ethylene binding energy, 21 kcal/mol, is substantially smaller than the calculated energies given in Table 1. The most obvious explanation for this difference is the quality of the basis set used. Previous Cp$_2$Zr−CH$_3^+$ studies used deficient basis sets on the cyclopentadienyl ligands assuming that it should not matter. It does matter. Using the B3LYP/6-31g* geometry, we find Cp$_2$Zr−CH$_3^+$ ethylene binding energies increase when poorer basis sets are used; see Table 8. The 6-31g* basis set results of Table 8 are certainly not the final "correct" answer as there are systematically larger basis sets that could be used. The inadequacy of even the 6-31g* basis is confirmed by the observation that the Cp$_2$Zr−OCH$_3^+$ ethylene complex binding energy has a 3 kcal/mol Boys−Bernardi basis set superposition error (BSSE).[124]

There have been a few computational studies that have examined the competition between olefin binding and counteranion binding including the study of olefin-separated ion pairs (OSIP). These data are collected in Table 9. Complexation energies are significantly dependent upon the counteranion; compare entries 2, 4, and 9. The dielectric effect of solvent can also have an impact; entries 1 and 10−15 included the effects of a dielectric continuum. Including a toluene solvent as a dielectric continuum appears to lower the endothermicity of olefin binding by ∼4 kcal/mol (compare entries 7−9 with entries 10−12). In all cases the counteranion effectively competes with the olefin. As shown by each of the insertion studies of section IV.D, olefin binding

Table 8. Electronic Structure Study of Olefin Binding[a]

	metric parameters				total energy	
compound	π complexation	M−C_α	M−C_β	ϕ	complexed	extended/ separated
$Cp_2ZrH^+ + C_2H_4$	22	2.82	2.84	90	−512.672284	−512.637200
$Cp_2ZrCH_3^+ + C_2H_4$	21	2.86	2.84	26	−551.989556	−551.956801
$Cp_2ZrOCH_3^+ + C_2H_4$	17	2.90	2.83	25	−627.267928	−627.240603
13, $n = 1$	11	2.84	2.95	26	−744.015772	−743.997525
13, $n = 2$	18	2.73	2.91	28	−783.337682	−783.309259
13, $n = 3$	15	2.73	2.99	25	−822.645784	−822.622199
X-ray, **16**, $n = 2$ (ref 119)		2.68(2)	2.89(2)	39.5/25.3		
$Cp_2ZrCH_3^+ + C_2H_4$ (4−31 g)	26				−551.351692	−551.310521
$Cp_2ZrCH_3^+ + C_2H_4$ (3-21 g)	30				−549.267483	−549.219884
$Cp_2ZrOCH_3^+ + C_2H_4$ (ghost)					−548.652223	−78.588260
$Cp_2ZrOCH_3^+ + C_2H_4$					−548.650801	−78.584920
$Cp_2ZrOCH_3^+ + C_2H_4$ (BSSE)	3				0.001422	0.00334

[a] B3LYP/6−31g* complexation energies (kcal/mol), distances (Å), angles (deg), and total energies for the complexed and extended/separated conformations (Hartrees).

Table 9. Ethylene Complexation Energies (kcal/mol) for Ion-Paired Complexes

	compound	method	π complexation	ref
1.	$(SiH_2CpNH)TiCH_3^+ \cdot CH_3B(C_6F_5)_3^- + C_2H_4$	MP2	∼0	38
2.	$Cp_2TiCH_3^+ \cdot Al(CH_3)_2Cl_2^- + C_2H_4$	CGA(PWB)	−28	19
3.	$Cp_2ZrCH_3^+ \cdot Al(CH_3)_2Cl_2^- + C_2H_4$	CGA(PWB)	−33	20
4.	$Cp_2TiCH_3^+ \cdot Cl_2Al[O(Al(CH_3)_3)AlMeH]_2^- + C_2H_4$	CGA(PWB)	−7	20
5.	$Cp_2ZrCH_3^+ \cdot Cl_2Al[O(Al(CH_3)_3)AlMeH]_2^- + C_2H_4$	CGA(PWB)	−9	20
6.	$Cp_2ZrCH_3^+ \cdot CH_3B(C_6F_5)_3^- + C_2H_4$	BLYP	−10	21
7.	$Cp\ Ti(CH_3)_2^+ \cdot CH_3B(C_6F_5)_3^- + C_2H_4$	GC-DFT	21	22
8.	$H_2SiCp(NH)Ti(CH_3)^+ \cdot CH_3B(C_6F_5)_3^- + C_2H_4$	GC-DFT	18	22
9.	$Cp_2TiCH_3^+ \cdot CH_3B(C_6F_5)_3^- + C_2H_4$	GC-DFT	10	22
10.	$Cp\ Ti(CH_3)_2^+ \cdot CH_3B(C_6F_5)_3^- + C_2H_4$	GC-DFT(TDC)	14	22
11.	$H_2SiCp(NH)Ti(CH_3)^+ \cdot CH_3B(C_6F_5)_3^- + C_2H_4$	GC-DFT(TDC)	14	22
12.	$Cp_2TiCH_3^+ \cdot CH_3B(C_6F_5)_3^- + C_2H_4$	GC-DFT(TDC)	6	22
13.	$Cp\ Zr(CH_3)_2^+ \cdot CH_3B(C_6F_5)_3^- + C_2H_4$	GC-DFT(TDC)	13	22
14.	$H_2SiCp(NH)Zr(CH_3)^+ \cdot CH_3B(C_6F_5)_3^- + C_2H_4$	GC-DFT(TDC)	10	22
15.	$Cp_2ZrCH_3^+ \cdot CH_3B(C_6F_5)_3^- + C_2H_4$	GC-DFT(TDC)	8	22

competes with ground-state agostic interactions, leading to their disruption. Not suprisingly, Lanza, Fragala, and Marks[18] computationally find that a counteranion effectively disrupts ground-state agostic interactions in the propyl product.

To survey the role of ion pairing in polymerization catalysis, the Rappé group has developed a MAO model based on structural studies by the Barron[125] and Roesky[126] groups, along with analogy to AlRNR′ clusters. This work led us to the proposal that MAO is a family of $(AlMeO)_n$ clusters containing an admixture of $AlMe_3$, the base unit being Barron's $(AlRO)_9$ cluster, shown in Figure 2 as **A**. $(AlRO)_9$ is composed of six-membered rings with strained four-membered rings adjacent to the ends or caps. Larger members of the family can be formed by addition reactions involving the strained four-membered rings. This model is consistent with the very recent minimal basis set DFT study of Zakharov and co-workers.[127] They computed large clusters/cages to be more stable than smaller ring structures. Zakharov and co-workers also found that reaction of these clusters/cages with Al_2Me_6 was exothermic.

The Al centers in the four-membered rings can be considered as "protected" or latent Lewis acid centers.[125] As shown in eq 12, reaction with a Lewis base

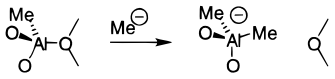

(12)

such as Me^- results in the conversion of a three-coordinate oxygen into a less strained two-coordinate oxygen. The two-coordinate oxygen can react with excess trimethylaluminum; see eq 13. If methyl abstraction occurs as outlined, all members of the family should react in the same manner and present the same basic shape to the cationic metal center. Thus, the Al_9 cluster was adopted as a MAO model (MAO_9).

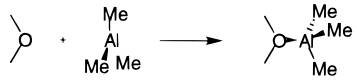

(13)

To evaluate the usefulness of this model, the barrier to methyl exchange (see eq 6) was computed for MAO_9 plus bis(1,2-dimethyl cyclopentadienyl)-zirconium cation. The computed barrier of 24 kcal/mol is in fair agreement with the experimental estimate of 18 kcal/mol.

For the MCP system, **13**, the reaction pathway from the transition state down to the product was investigated using the reaction potential model 1. Taking a 0.1 Å step along the imaginary frequency mode of the Hessian (the reaction coordinate) started the process. Newton−Raphson steps of 0.1 Å were taken until the product was attained. Parallel studies were carried out with and without MAO_9 present. Without the counteranion, the expected polymer chain flip pathway was followed. With the counter-

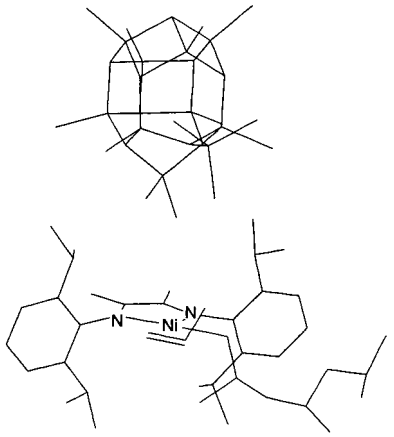

Figure 10. Ion pair model of Brookhart's nickel diimine polymerization catalyst. The lowest energy structure places the MAO9 counteranion over one of the square planar axial sites rather than in a position that competes with olefin for complexation.

anion present, the polymer reverted to its original position as the system progressed from the saddle point region down toward the product. The process was repeated for several anion positions. Inversion/retention differentiation was found to strongly depend on the initial anion position. This theoretical investigation suggests that, under experimental conditions where contact ion pairing is favored, the C_s-symmetric mono-Cp system will create isotactic polymer, and under experimental conditions where solvent separated ion pairing dominates, syndiotactic or atactic polymer will be formed. This computational observation is in accord with Shiomura's hypothesis that contact ion pairing prevents chain migratory insertion while permitting "chain stationary insertion".[118]

When MAO_9 was computationally added to **4,** Brookhart's diimine catalyst,[6,11] and a conformational search carried out, MAO_9 was found to sit over one of the two axial sites, not at the equatorial site used for olefin coordination; see Figure 10. This is in contrast to metallocenium systems wherein the anion and olefin must compete for binding site. If axial counteranion binding is correct for **4**, the counteranion will not compete with olefin for binding. A large olefin binding energy should be experimentally observed, and zeroth-order kinetics are a reasonable outcome. This model is also consistent with the similarity in reactivity between neutral and cationic Ni(II) catalysts, behavior which is in sharp contrast with that of neutral and cationic group 13 and 14 complexes.

C. Solvent Effects

If degree of ion pairing is an important differential factor in single-center polymerization, then ion pair solvation is also important. As discussed above, Deck and Marks[12,106a] find ion pair reorganization kinetics to be strongly influenced by the solvent. For the process depicted in eq 6 the free energy barrier is 16 kcal/mol in phenyl chloride and 19 kcal/mol in toluene. The similarity in free energy of activation masks a large enthalpy/entropy compensation effect. The $\Delta H^{\ddagger}$ values differ by 13 kcal/mol (24 and 11 kcal/mol, respectively), and the $\Delta S^{\ddagger}$ values differ by 32 eu (17 and −15 eu, respectively). For the polar solvent phenyl chloride, ion pair dissociation induces solvent organization and a positive entropy. For the nonpolar solvent toluene, ion pair dissociation leads to the usual negative translation and rotation entropy terms.

Table 10. Epimerization Data for *rac*-Ethylene-(4,5,6,7-tetrahydro-1-indenyl)zirconium[a]

$[C_3H_6]$ (mol/L)	[m]	$[C_3H_6]$ (mol/L)	[m]
0.35	0.62	1.1	0.84
0.7	0.76	3.8	0.92

[a] [m] is the fraction of *meso* dyads in the polymer (from ref 128a).

In addition to normal solvation effects, d^0 metal ions have been observed to bind aromatic rings such as in toluene. Eisch[15] has coined the term solvated cation−anion pairs (SCAP) to describe systems where a solvent disrupts an ion pair. There have been three reports on specific solvent binding. Fusco, Longo, Masi, and Garbassi[20] calculated benzene to form a 24 kcal/mol weaker SCAP or SSIP than ethylene. Lanza, Fragala, and Marks[18] computed a specific interaction with benzene to weaken ion pairing by 20 kcal/mol. Quite recently Chan, Vanka, Pye, and Ziegler[22] studied ion pair disruption by toluene. They found the energy of generating a toluene SSIP to range from −6 kcal/mol for $CpZr(CH_3)_2^+$ to +20 kcal/mol for $Cp_2TiCH_3^+$ for a set of six Ti− and Zr−MeB-$(C_6F_5)_3^-$ ion pairs.

D. Chain Isomerization

As mentioned in section VII.A a startling dependence of isotacticity on propylene concentration has been observed by Busico and co-workers,[128] Leclerc and Brintzinger,[104] and Resconi and co-workers;[130] representative data are collected in Table 10. The most likely explanation for this dependence is that the polymer chain end isomerizes after it is formed but before the next insertion event occurs, eq 14. Two

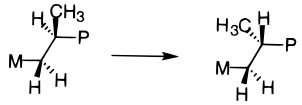

(14)

reaction sequences are plausible for this isomerization. The first involves a set of simple 1,2 H shifts, the first shift generating a tertiary alkyl chain, eq 15, and the second shift, eq 16, completing the isomerization, with stereochemical randomization.

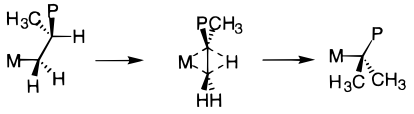

(15)

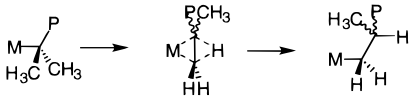

(16)

The second pathway[128c] involves a sequence of β-hydride elimination steps. The first β-hydride elimina-

Table 11. 1,2 Shift Data

	compound	method	barrier	*R*(C−H)	*R*(C−C)
1.	ethylene + H^+	B3LYP (cc-pVTZ)	−7	1.32	1.38
2.	ethylene + $H^\bullet$	B3LYP (cc-pVTZ)	42	1.29	1.49
3.	$Cp_2ZrC_2H_5^+$	BP DFT (DZVP) (ref 100)	31	1.31	1.37

tion is of the only β-hydrogen in a normal 1,2 insertion chain, eq 17. This is followed by rapid olefin rotation, eq 18, and olefin insertion to form a tertiary alkyl chain with equivalent methyl substituents, eq 19. A subsequent sequence of β-hydride elimination,

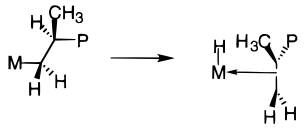

(17)

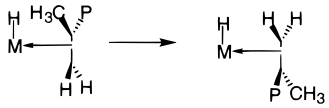

(18)

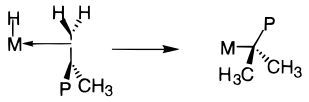

(19)

olefin rotation, and insertion steps would generate a 1,2 insertion chain of opposite stereochemistry. The β-hydride elimination, olefin rotation sequence has been invoked to explain the "chain walking" observed by Möhring and Fink for a nickel catalyst[130] and the isotopic scrambling observed in styrene hydrozirconation.[131] The computational data of section VI.A would argue against the viability of β-hydride elimination.

Both pathways, eqs 15 and 16 and eq 17−19, have been studied theoretically by Prosenc and Brintzinger[100] using DFT. They found the β-hydride elimination sequence to be preferred over the 1,2 shift pathway by 14 kcal/mol for an ethyl chain. They also calculated the β-hydride elimination sequence for propyl and isobutyl chains. The highest points along the β-hydride reaction sequence pathway dropped with increasing chain length from 17 to 12 to 10 kcal/mol for the ethyl, propyl, and isobutyl chains, respectively. Prosenc and Brintzinger concluded that the β-hydride reaction sequence is the operative epimerization pathway.

Prosenc and Brintzinger commented on the structural similarity between the 1,2 shift transition state and protonated ethylene. Structural and energetic data collected in Table 11 also suggest similarity with the saddle point for 1,2 shift in the ethyl radical. In light of the recently observed[131] role that the counteranion plays in the energetic preferences of carbocations, it would be interesting to repeat the Prosenc−Brintzinger study in the presence of a counteranion. The ethyl radical-like 1,2 shift barrier of the bare cation could change into an ethyl cation-like 1,2 shift in the presence of a counteranion.

VIII. Conclusions and Future Directions

Computational modeling procedures have been used to study virtually every facet of olefin polymerization for nearly all families of known catalysts. What have we learned from modeling?

Computational studies have generally supported, and have at times extended, "visual" models developed by experimentalists. Ideas extracted from theoretical studies such as the bonding model of Thorn and Hoffman[77] and Corradini's[3] recognition of the importance of the polymer chain have synergistically enhanced our understanding of the mechanisms of polymerization catalysis. This has led to more refined visual models which will lead to the development of new catalysts. The ultimate goal of computational modeling is, after all, to have an impact on real-world catalysts.

Over the past decade increasingly sophisticated technologies have been applied to olefin polymerization. Not too long ago optimizing the geometry of a simple zirconocene−ethylene complex by quantum mechanics was a heroic effort.[40] Today, quantum mechanical geometry optimizations of complexes containing more than 80 atoms are feasible.[46] In the euphoria of these accomplishments one must not lose sight of the need for proper calibration by comparison with experiment. Current state-of-the-art methodologies yield results that differ by more than 30 kcal/mol for the ethylene binding energy for the same complex. Ongoing efforts in the Marks,[12,106] Jordan,[119,133] Casey,[68,134] and Erker[135] groups are providing the precise energetic and structural data that will serve to provide proper validation for emerging theoretical methodologies. It seems certain that inclusion of the solvent and a counteranion as well as the dynamical effects of temperature will be necessary to reproduce these experimental data, yet only a few computational studies have been reported that account for counteranions as large as the 38-atom $CH_3B(C_6F_5)_3^-$ as well as the dielectric effect of solvent.

Computational models of regio- and stereoselectivity generally overestimate energy differences. Trends are reproduced, but magnitudes are exaggerated. Below we outline three sources of error.

(1) The 6−12 potential commonly used in molecular mechanics is intrinsically too stiff.[69b] Exponential-6, 6−12, and CI potentials for H_2 + He with precisely the same well depths and equilibrium distances are compared in Figure 11.[69b] Note the inner repulsive wall of the 6−12 potential rises too quickly.

(2) The lack of a dispersion term in modern density functional theory leads to a repulsive interaction between hydrocarbons.[136,137] B3LYP, 6-31g* MP2, and cc-pVQZ[138] MP2 methane dimer potential curves are collected in Figure 12. The cc-pVQZ B3LYP curve is purely repulsive due to the lack of dispersion. The 6-31g* MP2 curve has an attractive well, but because of angular limitations in the basis set, the well is too small. The cc-pVQZ MP2 curve is within 0.1 kcal/mol of the exact answer.

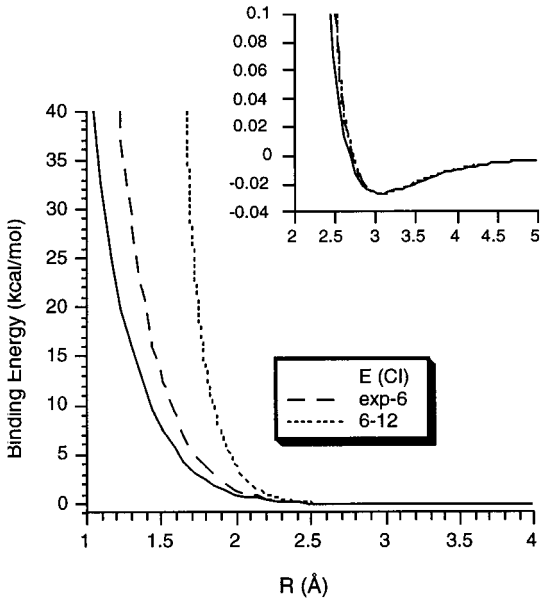

Figure 11. Methane dimer potential curves.

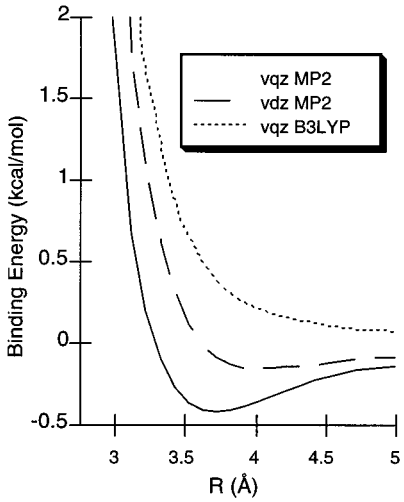

Figure 12. H_2 plus He potential curves.

(3) Virtually all studies of regio- and stereodifferentiation have kept the active atoms of the transition state fixed when the model is extended from a small QM model to an extended, more structurally realistic, molecular mechanics model. This restriction leads to an energetic overestimation because structural relaxation/optimization lowers the energy of a system. The more hindered the configuration, the more likely structural relaxation should occur, and the larger the constraint error.

In conclusion, we hope that the bare gas-phase cation computational model will soon join the use of Cl as a replacement for Cp[91,139] in the historical archives of theoretical chemistry. Both models have run their course. We look forward to the new insights gained from computational studies that include counteranions, solvent, and dynamical effects.

IX. Acknowledgment

We acknowledge financial support for this work from B. F. Goodrich, BP-Amoco, Exxon, Shell, and Union Carbide. We also acknowledge the intellectual contributions of our colleagues and current and former students and postdocs who have contributed to this effort, in particular L. M. Bormann-Rochotte, L. A. Castonguay, J. R. Hart, G. B. McGaughey, M. A. Pietsch, O. G. Polyakov, M. Win Gildenmeister, and D. C. Wiser.

X. References

(1) Montagna, A. A.; Dekmezian, A. H.; Burkhart, R. M. *Chemtech* **1997**, 26.
(2) Pino, P.; Cioni, P.; Wei, J. *J. Am. Chem. Soc.* **1987**, *109*, 6189.
(3) Corradini, F.; Guerra, G.; Vacatello, M.; Villani, V. *Gazz. Chim. Ital.* **1988**, *118*, 173.
(4) Ewen, J. A. *J. Mol. Catal., A* **1998**, *128*, 103.
(5) Schmidt, G. F.; Brookhart, M. *J. Am. Chem. Soc.* **1985**, *107*, 1443.
(6) Johnson, L. K.; Killian, C. M.; Brookhart, M. *J. Am. Chem. Soc.* **1995**, *117*, 6414.
(7) Brintzinger, H. H.; Fischer, D.; Mülhaupt, R.; Rieger, B.; Waymouth, R. *Angew. Chem., Int. Ed. Engl.* **1995**, *34*, 1143.
(8) Coates, G. W. *Chem. Rev.* **2000**, *100*, 1223.
(9) Alt, H. G.; Köppl, A. *Chem. Rev.* **2000**, *100*, 1205.
(10) Resconi, L. *Chem. Rev.* **2000**, *100*, 1253.
(11) Johnson, L. K.; Ittel, S. D.; Brookhart, M. *Chem. Rev.* **2000**, *100*, 1169.
(12) Chen, E. Y.-X.; Marks, T. J. *Chem. Rev.* **2000**, *100*, 1391.
(13) Britovsek, G. J. P.; Gibson, V. C.; Wass, D. F. *Angew. Chem., Int. Ed.* **1999**, *38*, 428.
(14) Angermund, K.; Fink, G.; Jensen, V. R.; Kleinschmidt, R. *Chem. Rev.* **2000**, *100*, 1457.
(15) Strauss, S. H. *Chem. Rev.* **1993**, *93*, 927.
(16) Chen, Y.-X.; Marks, T. J. *Organometallics* **1997**, *16*, 3649.
(17) (a) Eisch, J. J.; Caldwell, K. R.; Werner, S.; Krüger, C. *Organometallics* **1991**, *10*, 3417. (b) Eisch, J. J.; Pombrik, S. I.; Zheng, G.-X. *Organometallics* **1993**, *12*, 3856.
(18) Lanza, G.; Fragalá, I. L.; Marks, T. J. *J. Am. Chem. Soc.* **1998**, *120*, 8257.
(19) Fusco, R.; Longo, L.; Masi, F.; Garbassi, F. *Macromol. Rapid Commun.* **1997**, *18*, 433.
(20) Fusco, R.; Longo, L.; Proto, A.; Masi, F.; Garbassi, F. *Macromol. Rapid Commun.* **1998**, *19*, 257.
(21) Beck, S.; Prosenc, M. H.; Brintzinger, H. H. *J. Mol. Catal., A* **1998**, *128*, 41.
(22) Chan, M. S. W.; Vanka, K.; Pye, C. c.; Ziegler, T. *Organometallics* **1999**, *18*, 4624.
(23) Goodall, B. L. *J. Chem. Educ.* **1986**, *63*, 191.
(24) (a) Corradini, P.; Guerre, G.; Fusco, R.; Barone, V. *Eur. Polym. J.* **1980**, *16*, 835. (b) Corradono, P.; Busico, V.; Guerre, G. *Transition Metals and Organometallics as Catalysis for Olefin Polymerization*; Springer-Verlag: Berlin, 1988; p 337. (c) Corradini, P.; Barone, V.; Fusco, R.; Guerra, G. *J. Catal.* **1982**, *77*, 32. (d) Corradini, P.; Guerra, G.; Barone, V. *Eur. Polym. J.* **1984**, *20*, 1177. (e) Venditto, V.; Guerra, G.; Corradini, P. *Eur. Polym. J.* **1991**, *27*, 45.
(25) (a) Cossee, P. *J. Catal.* **1964**, *3*, 80. (b) Arlman, E. J.; Cossee, P. *J. Catal.* **1964**, *3*, 99.
(26) Flory, P. J. *Principles of Polymer Chemistry*; Cornell University Press: Ithaca, NY, 1953; p 317.
(27) Reid, R. C.; Prausnitz, J. M.; Poling, B. E. *The Properties of Gases and Liquids*, 4th ed.; McGraw-Hill: New York, 1987.
(28) Stehling, U.; Diebold, J.; Kirsten, R.; Röll, W.; Brintzinger, H. H.; Jüngling, S.; Mülhaupt, R.; Langhauser, F. *Organometallics* **1994**, *13*, 964.
(29) (a) Spaleck, W.; Küber, F.; Winter, A.; Rohrmann, J.; Bachmann, B.; Antberg, M.; Dolle, V.; Paulus, E. F. *Organometallics* **1994**, *13*, 954. (b) Spaleck, W.; Küber, F.; Bachmann, B.; Fritze, C.; Winter, A. *J. Mol. Catal., A* **1997**, *128*, 279.
(30) Coates, G. W.; Waymouth, R. M. *Science* **1995**, *267*, 217.
(31) Kaminsky, W.; Külper, K.; Brintzinger, H. H.; Wild, F. R. W. P. *Angew. Chem., Int. Ed. Engl.* **1985**, *24*, 507.
(32) Rappé, A. K.; Casewit, C. J. *Molecular Mechanics Across Chemistry*; University Science Books: Sausalito, CA, 1997.
(33) Erker, G.; Nolte, R.; Aul.; R.; Wilker, S.; Krüger, C.; Noe, R. *J. Am. Chem. Soc.* **1991**, *113*, 7594.
(34) Yu, Z.; Chien, J. C. W. *J. Poly. Sci., A* **1995**, *33*, 125.
(35) Cavallo, L.; Guerra, G. *Macromolecules* **1996**, *29*, 2729.
(36) Fait, A.; Resconi, L.; Guerra, G.; Corradini, P. *Macromolecules* **1999**, *32*, 2104.
(37) Guerra, G.; Longo, P.; Cavallo, L.; Corradini, P.; Resconi, L. *J. Am. Chem. Soc.* **1997**, *119*, 4394
(38) Bormann-Rochotte, L. M. Molecular Modeling Applied to an Isotactic Polypropylene Catal. Diss. Abstr. Int., B **1998**, *59*, 2228; CAN 129:260917. Bormann-Rochotte, L. M.; Rappé, A. K. Manuscript in preparation.
(39) Hehre, W. J.; Radom, L.; v.R. Schleyer, P.; Pople, J. A. *Ab Initio Molecular Orbital Theory*; Wiley-Interscience: New York, 1986.

(40) Jolly, C. A.; Marynick D. S. *J. Am. Chem. Soc.* **1989**, *111*, 7968.
(41) Natta, G.; Pino, P.; Mazzanti, G.; Giannini, U. *J. Am. Chem. Soc.* **1957**, *79*, 2975. Breslow, D. S.; Newberg, N. R. *J. Am. Chem. Soc.* **1957**, *79*, 5072.
(42) Wild, F. R. W. P.; Zsolnai, L.; Huttner, G.; Brintzinger, H. H. *J. Organomet. Chem.* **1982**, *2332*, 233. Ewen, J. A. *J. Am. Chem. Soc.* **1984,** *106*, 6355.
(43) (a) Musaev, D. G.; Froese, R. D. J.; Svensson, M.; Morokuma, K. *J. Am. Chem. Soc.* **1997**, *119*, 367. (b) Musaev, D. G.; Svensson, M.; Morokuma, K. *Organometallics* **1997**, *16*, 1933.
(44) Deng, L.; Margl, P.; Ziegler, T. *J. Am. Chem. Soc.* **1997**, **119**, 1094;
(45) (a) Britovsek, G. J. P.; Gibson, V. C.; Kimberley, B. S.; Maddox, P. J., McTavish, S. J.; Solan, G. A.; White, A. J. P.; Williams, D. J. *Chem. Commun.* **1998**, 849. (b) Small, B. L.; Brookhart, M. *J. Am. Chem. Soc.* **1998**, *120*, 7143.
(46) Griffiths, E. A. H.; Britovsek, G. J. P.; Gibson, V. C.; Gould I. R. *Chem. Commun.* **1999** 1333.
(47) Deng, L.; Margl, P.; Ziegler, T. *J. Am. Chem. Soc.* **1999**, *121*, 6479.
(48) Svensson, M.; Humbel, S.; Froese, R. D. J.; Matsubara, T.; Sieber, S.; Morokuma, K. *J. Phys. Chem.* **1996**, *100*, 19357.
(49) Woo, T. K.; Cavallo, L.; Ziegler, T. *Theor. Chem. Acc.* **1998**, *100*, 307.
(50) Rappe, A. K.; Pietsch, M. A.; Wiser, D. C.; Hart, J. R.; Bormann-Rochotte, L. M.; Skiff, W. M. *Mol. Eng.* **1997**, *7*, 385.
(51) Pietsch, M. A.; Rappe, A. K. *Book of Abstracts*, 212th ACS National Meeting, Orlando, FL, Aug 25−29, 1996; American Chemical Society: Washington, DC, 1996; AN 1996:413403. Pietsch, M. A.; Rappe, A. K. *Polym. Mater. Sci. Eng.* **1996**, *74* 420.
(52) Deng, L.; Woo, T. K.; Cavallo, L.; Margl, P. M.; Ziegler, T. *J. Am. Chem. Soc.* **1997**, *119*, 6177.
(53) (a) Froese, R..J.; Musaev, D. G.; Morokuma, K. *J. Am. Chem. Soc.* **1998**, *120*, 1581. (b) Musaev, D. G.; Froese, R. D. J.; Morokuma, K. *Organometallics* **1998**, *17*, 1850.
(54) Froese, R. D. J.; Musaev, D. G.; Morokuma, K. *Organometallics* **1999**, *18*, 373.
(55) Collman, J. P.; Hegedus, L. S.; Norton, J. R.; Finke, R. G. *Principles and Applications of Organotransition Metal Chemistry*; University Science Books: Mill Valley, CA, 1987.
(56) Woo, T. K.; Fan, L.; Ziegler *Organometallics* **1994**, *13*, 432. Woo, T. K.; Fan, L.; Ziegler, T. *Organometallics* **1994**, *13*, 2252.
(57) Fujimoto, H.; Yamasaki, T.; Mizutani, H.; Koga, N. *J. Am. Chem. Soc.* **1985**, *107*, 6157.
(58) Kawamura-Kuribayashi, H.; Koga, N.; Morokuma, K. *J. Am. Chem. Soc.* **1992**, *114*, 2359.
(59) Kawamura-Kuribayashi, H.; Koga, N.; Morokuma, K. *J. Am. Chem. Soc.* **1992**, *114*, 8687.
(60) Yoshida, T.; Koga, N.; Morokuma K. *Organometallics* **1995**, *14*, 746.
(61) Jensen, V. R.; Børve, K. J. *Organometallics* **1997**, *16*, 2514.
(62) Axe, F. U.; Coffin, J. M. *J. Phys. Chem.* **1994**, *98*, 2567.
(63) Bernardi, F.; Bottoni, A.; Miscione, G. P. *Organometallics* **1998**, *17*, 16.
(64) Fusco, R.; Longo, L.; Masi, F.; Garbassi, F. *Macromolecules* **1997**, *30*, 7673.
(65) Deng, L.; Ziegler, T.; Woo, T. K.; Margl, P.; Fan, L. *Organometallics* **1998**, *17*, 3240.
(66) (a) Brookhardt, M.; Green, M. L. H. *J. Organomet. Chem.* **1983**, *250*, 395. (b) Brookhart, M.; Green, M. L. H.; Wong, L.-L. *Prog. Inorg. Chem.* **1988**, *36*, 1.
(67) Grubbs, R. H.; Coates, G. W. *Acc. Chem. Res.* **1996**, *29*, 85.
(68) Casey, C. P.; Hallenbeck, S. L.; Pollock, D.W.; Landis, C. R. *J. Am. Chem. Soc.* **1997**, *117*, 9770. Casey, C. P.; Hallenbeck, S. L.; Wright, J. M.; Landis, C. R. *J. Am. Chem. Soc.* **1997**, *119*, 9680.
(69) (a) Cornell, W. D.; Cieplak, P.; Bayly, C. I.; Gould, I. R.; Merz, K. M., Jr.; Ferguson, D. M.; Spellmeyer, D. C.; Fox, T.; Caldwell, J. W.; Kollman, P. A. *J. Am. Chem. Soc.* **1995**, *117*, 5179. (b) Hart, J. R.; Rappé, A. K. *J. Chem. Phys.* **1992**, *97*, 1109.
(70) Upton, T. H.; Rappé, A. K. *J. Am. Chem. Soc.* **1985**, *107*, 1206. Rappé, A. K. *Organometallics*, **1987**, *6*, 354. 37. Rappé, A. K. Upton, T. H. *J. Am. Chem. Soc.* **1992**, *114*, 7507.
(71) Woodward, R. B.; Hoffmann, R. *The Conservation of Orbital Symmetry*; Verlag Chemie: Weinheim/Bergstrasse, 1970.
(72) Gonzalez, C.; Sosa, C.; Schlegel, N. B. *J. Phys. Chem.* **1989**, *93*, 2435. Gonzalez, C.; McDouall, J. J. W.; Schlegel, H. B. *J. Phys. Chem.* **1990**, *94*, 7467.
(73) Rowley, D.; Steiner, H. *Discuss. Faraday Soc.* **1951**, *10*, 198.
(74) Doering, W. von E.; Toscano, V. G.; Beasley, G. H. *Tetrahedron* **1971**, *27*, 5299.
(75) Armstrong, D. R.; Perkins, P. G.; Stewart, J. J. P. *J. Chem. Soc., Dalton Trans.* **1972**, 1972.
(76) Lauher, J. W.; Hoffmann, R. *J. Am. Chem. Soc.* **1976**, *98*, 1729.
(77) Thorn, D. L.; Hoffman, R. *J. Am. Chem. Soc.* **1978**, *100*, 2079.
(78) Novaro, O.; Blaisten-Barojas, E.; Clementi, E.; Giunchi, G.; Ruiz-Vizcaya, M. E. *J. Chem. Phys.* **1978**, *68*, 2337.
(79) Fujimoto, H.; Yamasaki, T.; Mizutani, H.; Koga, N. *J. Am. Chem. Soc.* **1985**, *107*, 6157.
(80) Koga, N.; Obara, S.; Kitaura, K.; Morokuma, K. *J. Am. Chem. Soc.* **1985**, *107*, 7109.
(81) Koga, N.; Morokuma, K. *Chem. Rev.* **1991**, *91*, 823. Kawamura-Kuribayashi, H.; Koga, N.; Morokuma, K. *J. Am. Chem. Soc.* **1992**, *114*, 2359.
(82) Resconi, L.; Piemontesi, F.; Camurati, I.; Sudmeijer, O.; Nifant′ev, I. E.; Ivchenko, P. V.; Kuz′mina, L. G. *J. Am. Chem. Soc.* **1998**, *120*, 2308.
(83) Ewen, J. A.; Jones, R. L.; Razavi, A. *J. Am. Chem. Soc.* **1988**, *110*, 6255.
(84) Castonguay, L. A.; Rappé, A. K. *J. Am. Chem. Soc.* **1992**, *114*, 4. 5832.
(85) Hart, J. R.; Rappé, A. K. *J. Am. Chem. Soc.* **1993**, *115*, 6159.
(86) Kawamura-Kuribayashi, H.; Koga, N.; Morokuma, K. *J. Am. Chem. Soc.* **1992**, *114*, 8687.
(87) Yoshida, T.; Koga, N.; Morokuma, K. *Organometallic* **1996**, *15*, 766.
(88) Cavallo, L.; Guera, G.; Vacatello, M.; Corradini, P. *Macromolecules* **1991**, *24*, 1784.
(89) Jolly, C. A.; Marynick, D. S. *Inorg. Chem.* **1989**, *28*, 2893.
(90) Bierwagen, E. P.; Bercaw, J. E.; Goddard, W. A., III. *J. Am. Chem. Soc.* **1994**, *116*, 1481.
(91) Rappé, A. K.; Goddard, W. A., III. *J. Am. Chem. Soc.* **1982**, *104*, 297.
(92) Yang, X.; Stern, C. L.; Marks, T. J. *J. Am. Chem. Soc.* **1991**, *113*, 3623.
(93) Pietsch, M. A.; Rappé, A. K. J. *Am. Chem. Soc.* **1996**, *118*, 10908.
(94) Golab, J. T. *Chemtech* **1998**, 17.
(95) Schneider, M. J.; Suhm, J.; Mülhaupt, R.; Prosenc, M. H.; Brintzinger, H. H. *Macromolecules* **1997**, *30*, 3164.
(96) Watson, P. L.; Roe. D. C.*J. Am. Chem. Soc.* **1982**, *104*, 6471.
(97) Resconi, L.; Piemontesi, F.; Franciscono, G.; Abis, L.; Fiorani, T. *J. Am. Chem. Soc.* **1992**, *114*, 1025.
(98) Busfield, W. Heats and Entropies of Polymerization, Ceiling Temperatures, Equilibrium Monomer Concentrations and Polymerizability of Heterocyclic Compounds. In *Polymer Handbook*, 3rd ed.; Brandrup, K. J., Immergut, E. H., Eds.; J. Wiley & Sons: New York, 1989; p II/297.
(99) (a) Lohrenz, J. C. W.; Wood, T. K.; Fan, L. Ziegler, T. *J. Organomet. Chem.* **1995**, *497*, 91. (b) Margl, P.; Deng, L.; Ziegler, T. *Organometallics*, **1999**, *17*, 933. (c) Margl, P.; Deng, L.; Ziegler, T. *J. Am. Chem. Soc.* **1999**, *120*, 5517. (d) Margl, P.; Deng, L.; Ziegler, T. *J. Am. Chem. Soc.* **1999**, *120*, 154.
(100) Prosenc, M.-H.; Brintzinger, H-.H. *Organometallics* **1997**, *16*, 3889.
(101) Clawson, L.; Soto, J.; Buchwald, S. L.; Steigerwald, M. L. *J. Am. Chem. Soc.* **1985**, *107*, 3377.
(102) Piers, W. E.; Bercaw, J. E. *J. Am. Chem. Soc.* **1990**, *112*, 9406.
(103) Krauledat, H.; Brintzinger, H.-H. *Angew. Chem., Int. Ed. Engl.* **1990**, *29*, 1412.
(104) Leclerc, M. K.; Brintzinger, H. H. *J. Am. Chem. Soc.* **1995**, *117*, 1651. Leclerc, M. K.; Brintzinger, H. H. *J. Am. Chem. Soc.* **1996**, *118*, 9024.
(105) Jordan, R. F.; Bajgur, C. S.; Willett, R.; Scott, B. *J. Am. Chem. Soc.* **1986**, *108*, 7410.
(106) (a) Deck, P. A.; Marks, T. J. *J. Am. Chem. Soc.* **1995**, *117*, 6128. (b) Chen, Y.-X.; Stern, C. L.; Marks, T. J. *J. Am. Chem. Soc.* **1997**, *119*, 2582. (c) Deck, P. A.; Beswick, C. L.; Marks, T. J. *J. Am. Chem. Soc.* **1998**, *120*, 1772.
(107) (a) Siedle, A. R.; Lamanna, W. M.; Newmark, R. A.; Stevens, J.; Richardson, D. E.; Ryan, M. *Makromol. Chem., Macromol. Symp.* **1993**, *66*, 215. (b) Siedle, A. R.; Newmark, R. A. *J. Organomet. Chem.* **1995**, *497*, 119. (c) Siedle, A. R.; Hanggi, B.; Newmark, R. A. *Macromol. Symp.* **1995**, *89*, 299.
(108) Hahn, S.; Fink, G. *Macromol. Rapid Commun.* **1997**, *18*, 117.
(109) (a) Chien, J. C. W.; Tsai, W.-M.; Rausch, M. D. *J. Am. Chem. Soc.* **1991**, *113*, 8570−8571. (b) Vizzini, J. C.; Chien, J. C. W.; Babu, G. N.; Newmark, R. A. *J. Polym. Sci., Part A: Polym. Chem.* **1994**, *32*, 2049. (c) Chien, J. C. W.; Song, W.; Rausch, M. D. *J. Polym. Sci., Part A: Polym. Chem.* **1994**, *32*, 2387.
(110) Prosenc, M. H.; Janiak, C.; Brintzinger, H. H. *Organometallics* **1992**, *11*, 4036.
(111) Wiser, D. C. A Theoretical Investigation of Several Organometallic Transition States, 1995; CAN 124:176497. Wiser, D. C.; Rappé, A. K. *Book of Abstracts*, 211th ACS National Meeting, New Orleans, LA, March 24−28 1996; American Chemical Society: Washington, DC, 1996; AN 1996:221727. Wiser, D. C.; Rappé, A. K. *Polym. Mater. Sci. Eng.* **1996**, *74*, 423.
(112) The Zr−C bond distances in olefin complexes have in general been computed to be asymmetric. The Zr−C bond distances in the one observed olefin complex (ref 119) are also inequivalent. If one assumes that the closer C is bonded to Zr and the one further away not bonded, then a Zr−C nonbond distance can be estimated by averaging the longer of the two Zr−C ethylene bond distances for the eight zirconium ethylene structures of Table 1 and the six from Table 8; this yields a Zr−C nonbond distance of 2.86 Å. For reference the longer of the two olefin bond

distances in the single reported zirconium(IV) olefin complex is 2.89 Å (ref 119).
(113) Orpen, A. G.; Brammer, L.; Allen, F. H.; Kennard, O.; Watson, D. G.; Taylor, R. *J. Chem. Soc., Dalton Trans.* **1989**, S1.
(114) Shapiro, P. J.; Bunel, E.; Schaefer, W. P.; Bercaw J. E. *Organometallics* **1990**, *9*, 867. Shapiro, P. J.; Cotter, W. D.; Schaefer, W. P.; Labinger, J. A.; Bercaw J. E. *J. Am. Chem. Soc.* **1994**, *116*, 4623.
(115) Canich, J. A. M. (Exxon). U.S. Patent 5026798, 1991.
(116) Stevens, J. C.; Timmers, F. J.; Wilson, D. R.; Schmidt, G. F.; Nickias, P. N.; Rosen, R. K. Knight, G. W.; Lai, S.-Y. (Dow Chemical Co.) Eur. Pat. Appl. 0 416 815 A1, 1990. LaPointe, R. E.; Stevens, J. C.; Nickias, P. N.; McAdon, M. H. (Dow Chemical Co,) Eur. Pat. Appl. 0 520 732 A1, 1992.
(117) McKnight, A. L.; Masood, M. A.; Waymouth, R. M. *Organometallics* **1997**, *16*, 2879.
(118) Shiomura, T.; Asanuma, T.; Inoue, N. *Macromol. Rapid Commun.* **1996**, *17*, 9.
(119) Wu, Z.; Jordan, R. F.; Petersen, J. L *J. Am. Chem. Soc.* **1995**, *117*, 5867.
(120) Becke, A. D. *J. Chem. Phys.* **1993**, *98*, 5648.
(121) Ditchfield, R.; Hehre, W. J.; Pople, J. A. *J. Chem. Phys.* **1971**, *54*, 724. Hehre, W. J.; Ditchfield, R.; Pople, J. A. *J. Chem. Phys.* **1972**, *56*, 2257. Binkley, J. S.; Pople, J. A.; Hehre, W. J. *J. Am. Chem. Soc.* **1980**, *102*, 939.
(122) Hay, P. J.; Wadt, W. R. *J. Chem. Phys.* **1985**, *82*, 299.
(123) Gaussian 98, Revision A.6: Frisch, M. J.; Trucks, G. W.; Schlegel, H. B.; Scuseria, G. E.; Robb, M. A.; Cheeseman, J. R.; Zakrzewski, V. G.; Montgomery, Jr., J. A.; Stratmann, R. E.; Burant, J. C.; Dapprich, S.; Millam, J. M.; Daniels, A. D.; Kudin, K. N.; Strain, M. C.; Farkas, O.; Tomasi, J.; Barone, V.; Cossi, M.; Cammi, R.; Mennucci, B.; Pomelli, C.; Adamo, C.; Clifford, S.; Ochterski, J.; Petersson, G. A.; Ayala, P. Y.; Cui, Q.; Morokuma, K.; Malick, D. K.; Rabuck, A. D.; Raghavachari, K.; Foresman, J. B.; Cioslowski, J.; Ortiz, J. V.; Stefanov, B. B.; Liu, G.; Liashenko, A.; Piskorz, P.; Komaromi, I.; Gomperts, R.; Martin, R. L.; Fox, D. J.; Keith, T.; Al-Laham, M. A.; Peng, C. Y.; Nanayakkara, A.; Gonzalez, C.; Challacombe, M.; Gill, P. M. W.; Johnson, B.; Chen, W.; Wong, M. W.; Andres, J. L.; Gonzalez, C.; Head-Gordon, M.; Replogle, E. S.; Pople, J. A. Gaussian, Inc., Pittsburgh, PA, 1998.
(124) Boys, S. F.; Bernardi, F. *Mol. Phys.* **1970**, *19*, 553.
(125) (a) Harlan, C. J.; Bott, S. G.; Barron, A. R. *J. Am. Chem. Soc.* **1995**, *117*, 6465−6474. (b) Mason, M. R.; Smith, J. M.; Bott, S. G.; Barron, A. R. *J. Am. Chem. Soc.* **1993**, *115*, 4971−4984.
(126) Storre, J.; Schnitter, C.; Roesky, H. W.; Schmidt, H.-G.; Noltemeyer, M.; Fleischer, R.; Stalke, Dietmar. *J. Am. Chem. Soc.* **1997**, *119*, 7504−7513.
(127) Zakharov, I. I.; Zakharov, V. A.; Porapov, A. G.; Zhiedomirov, G. M. *Macromol. Theory Simul.* **1999**, *8*, 272.
(128) (a) Busico, V.; Cipullo, R. *J. Am. Chem. Soc.* **1994**, *116*, 9329. (b) Busico, V.; Caporaso, L.; Cipullo, R.; Landriani, L. *J. Am. Chem. Soc.* **1996**, *118*, 2105. (c) Busico, V.; Cipullo, R.; Caporaso, L.; Angelini, G.; Segre, A. L. *J. Mol. Catal., A* **1998**, *128*, 53.
(129) Resconi, L.; Fait, A.; Piemontesi, F.; Colonnesi, M. *Macromolecules* **1995**, *28*, 6667.
(130) Möhring, V. M.; Fink, G. *Angew. Chem., Int. Ed. Engl.* **1985**, *24*, 1001.
(131) Nelson, J. E.; Bercaw, J. E.; Labinger, J. A. *Organometallics* **1989**, *8*, 2484.
(132) Fãrcasiu, D.; Hâncu, D. *J. Am. Chem. Soc.* **1999**, *121*, 7173.
(133) Jordan, R. F.; Carpentier, J. F.; Wu, Z.; Lee, C. W.; Christopher, J. N.; Stromberg, S.; Maryin, V. P. *Book of Abstracts*, 218th ACS National Meeting, New Orleans, LA, Aug 22−26, 1999; American chemical Society: Washington, DC, 1999; AN 1999:541780.
(134) Casey, C. P.; Fisher, J. J.; Fagan, M. A. *Book of Abstracts*, 218th ACS National Meeting, New Orleans, LA, Aug 22−26, 1999; American Chemical Society: Washington, DC, 1999; AN 1999: 541785.
(135) Karl, J.; Dahlmann, M.; Erker, G.; Bergander, K. *J. Am. Chem. Soc.* **1998**, *120*, 5643. Dahlmann, M.; Erker, G.; Nissinen, M.; Fröhlich, R. *J. Am. Chem. Soc.* **1999**, *121*, 2820. Erker, G.; Dahlman, M.; Fröhlich, R. *Book of Abstracts*, 218th ACS National Meeting, New Orleans, LA, Aug 22−26, 1999; American Chemical Society: Washington, DC, 1999; AN 1999:541759.
(136) Meijer, E. J.; Sprik, M. *J. Chem. Phys.* **1996**, *105*, 8684. Tsuzuki, S.; Uchimaru, T.; Tanabe, K. *Chem. Phys. Lett.* **1998**, *287*, 202.
(137) Rappé, A. K.; Bernstein, E. R. *J. Phys. Chem.*, submitted for publication.
(138) Dunning, T. H., Jr. *J. Chem. Phys.* **1989**, *90*, 1007. Kendall, R. A.; Dunning, T. H., Jr.; Harrison, R. J. *J. Chem. Phys.* **1992**, *96*, 6796. Woon, D. E.; Dunning, T. H., Jr. *J. Chem. Phys.* **1993**, *98*, 1358.
(139) Rappé, A. K. Theoretical studies of homogeneous catalysis by transition metal complexes, 1981; CAN 96:5945; AN 1982:59.

CR9902493